## This is the author's peer reviewed, accepted manuscript. However, the online version of record will be different from this version once it has been copyedited and typeset. PLEASE CITE THIS ARTICLE AS DOI: 10.1063/5.0139558

## Surface transformations of electrocatalysts during the oxygen evolution reaction

Molly E. Vitale-Sullivan, Alvin Chang, Kuan-Hsun Chou, Zhenxing Feng, Kelsey A. Stoerzinger<sup>2, 3, a)</sup>

<sup>1</sup>School of Mechanical, Industrial, and Manufacturing Engineering, Oregon State University, Corvallis, Oregon 97331, USA

<sup>2</sup>School of Chemical, Biological, and Environmental Engineering, Oregon State University, Corvallis, Oregon 97331, USA

<sup>3</sup>Physical and Computational Sciences Directorate, Pacific Northwest National Laboratory, Richland, Washington 99354, USA

a) Author to whom correspondence should be addressed: zhenxing.feng@oregonstate.edu, kelsey.stoerzinger@oregonstate.edu

## I. ABSTRACT

Electrochemical water splitting (electrolysis)—driven by renewable electricity—offers a sustainable route for energy storage in hydrogen. Significant research has been undertaken to catalyze the kinetically hindered oxidation half reaction in water electrolysis, the oxygen evolution reaction (OER), with most studies focusing on improving electrocatalytic activity of OER. However, dynamic transformations of electrocatalyst surfaces during OER pose a challenge for understanding the intrinsic active sites. In this review, detection methods for surface transformations including electron microscopy, vibration spectroscopy, core level spectroscopy, and x-ray diffraction-based methods are discussed. Novel *in situ* and *operando* surface science techniques, multimodal characterization, and systematic experimental design will provide insight into the true active surface and OER mechanisms. Knowledge of electrocatalyst surface transformation pathways will lay the foundation for engineering pre-catalyst materials for scalable water electrolysis and support a sustainable energy future.

PLEASE CITE THIS ARTICLE AS DOI: 10.1063/5.0139558

## II. INTRODUCTION

Water electrolysis is a promising route for producing sustainable hydrogen for industrial, agricultural, transportation, and residential applications. At scale, renewably-powered water electrolysis could mitigate the high volume of CO<sub>2</sub> emissions from hydrogen production methods such as steam reforming of methane and coal gasification. The sluggish reaction kinetics of the anodic oxygen evolution reaction (OER) represent the largest source of efficiency loss (or overpotential) in the overall water electrolysis process.<sup>2, 3</sup> As a result, there have been intense efforts to develop highly active OER electrocatalysts<sup>4</sup> that are further stable,<sup>5</sup> selective,<sup>6</sup> earthabundant,<sup>3</sup> and economical.<sup>7</sup>

The OER is a heterogeneous reaction wherein inner-sphere electron transfer processes occur at the electrocatalyst-electrolyte interface.8 The associated rate constants of individual reaction steps depend on the chemical and structural nature of the electrocatalyst surface during the reaction.9 The significant overpotentials required to drive OER subjects electrocatalysts to highly oxidizing conditions that usually differ from those of traditional electrocatalyst synthesis. Therefore, it is reasonable to presume that polarized electrocatalyst surfaces might differ from their pristine state. Thus, the measured current density—proportional to activity—cannot be described solely by ex situ characterization of the pristine material but is instead linked to the electrocatalyst surface at a given applied potential. At the fundamental level, the intrinsic electrocatalyst activity (or the activity per active site) is of key importance when considering accurate electrocatalyst benchmarking. The possibility of electrocatalyst surface reconstruction during OER makes normalization of electrocatalytic current nontrivial and can lead to inconsistent comparisons in the context of existing literature. 10 Understanding the causes of material transformations—together with elucidating the true active sites and self-consistent reaction mechanisms—will advance the rational design of OER electrocatalysts.

PLEASE CITE THIS ARTICLE AS DOI: 10.1063/5.0139558

Over the past several decades, persistent efforts have been made to understand the OER mechanism, yet the electrocatalyst surface under oxidizing OER conditions remains poorly understood. 11 An increased interest in surface transformations of OER electrocatalysts arose after the discovery that the perovskite  $Ba_{0.5}Sr_{0.5}Co_{0.8}Fe_{0.2}O_{3-\delta}$  (abbreviated hereafter as BSCF82) undergoes surface amorphization during OER in alkaline media (KOH), accompanied by a dramatic four-fold increase in activity. 12 Transmission electron micrographs of the BSCF82 surface before and after OER showed a loss of A-site Ba and Sr cations, as well as a change in octahedral connectivity of the 20-100 nm surface layer, <sup>13</sup> providing compelling evidence that the increased OER activity is linked to surface transformation. Since the study of BSCF82 by May et al. (2012), many researchers acknowledge that the surface of OER electrocatalysts may transform under dynamic electrochemical conditions.<sup>12</sup>

In 2016, Seitz et al. demonstrated surface transformations of perovskites also occur in acidic media. Approximately  $\sim 30\text{-}50\%$  of the  $\text{Sr}^{2+}$  leached from the surface of  $\text{SrIrO}_3$  into the electrolyte during the first 30 min. of cycling (inductively coupled plasma optical emission spectroscopy), leaving behind an Ir-rich surface two orders of magnitude more active than rutile IrO<sub>2</sub>.<sup>14</sup> Density functional theory calculations indicated that possible transformed overlayer structures were anatase IrO2 or IrO3.14

Surface transformations of Ir-based double perovskites also provide a foundational understanding of OER electrocatalyst surface transformations in acidic media. Diaz-Morales et al. (2016) found that Ir-based double perovskites Ba<sub>2</sub>MIrO<sub>6</sub> (M = Y, La, Ce, Pr, Nd, Tb) generally transformed into Ir-rich surfaces with loss of Ba and M cations. 15 Both SrIrO<sub>4</sub> (consisting of 2D perovskite and SrO rock salt layers) and Pr<sub>3</sub>IrO<sub>7</sub> (forming 1D IrO<sub>6</sub> octahedral chains) were unstable during galvanostatic testing in acid compared to the highly active and stable 3D perovskite

PLEASE CITE THIS ARTICLE AS DOI: 10.1063/5.0139558

structures (Ba<sub>2</sub>YIrO<sub>6</sub> and Ba<sub>2</sub>PrIrO<sub>6</sub>).<sup>15</sup> Thus, the initial structure of the Ir-based double perovskites—a network of corner-sharing BO<sub>6</sub> octahedra—is crucial for resultant activity and surface stability.

While many of the early studies focus on surface transformations of perovskite oxides, more recent literature explores surface changes on other types of materials. To probe these complex surface dynamics, experimental measurements must reflect the environment of OER reaction conditions with high spatial and temporal resolution. Understanding dynamic electrocatalyst surfaces using *in situ* and *operando* characterization techniques will aid in determining the origin of electrocatalytic activity.

Herein, we refer to electrocatalyst transformations broadly as the physical, chemical, or electronic changes occurring on an electrocatalyst surface during OER. Both reversible and irreversible transformation processes have been reported in the literature. Changing the electrochemical potential at the electrocatalyst-electrolyte interface drives the pristine surface out of its original state, charges the electric double layer, and can induce (non-)Faradaic reactions. Material transformations have been found to differ widely depending on the pristine electrocatalyst structure/composition and electrocatalytic conditions, varying from strictly surface changes (<2 nm) to long-range transformation of the entire electrocatalyst material [Fig. 1(a)]. However, such changes are—at least in part—dynamic in nature and might be limited to only the terminal crystallographic plane, making them exceptionally challenging to characterize. While the magnitude of such transformation is by no means ubiquitous, many highly active OER electrocatalysts have been observed to exhibit changes in structure and composition after cycling, for the property of the structure and composition after cycling, for the property of the property of the property of the property of activity as well. The property of the property of activity as well. The property of activity and the property of activity and the property of activity. Bulk material electronic and



PLEASE CITE THIS ARTICLE AS DOI: 10.1063/5.0139558

surfaces.29

structural descriptors can not only guide electrocatalyst design, but also guide our understanding of likely surface transformations under oxidizing conditions. Many of these are inherently linked to electronic properties of electrocatalysts used to describe OER activity [Fig. 1(b)] including dband theory,<sup>24</sup> filling of the e<sub>g</sub> orbital of surface transition metal cations,<sup>25</sup> high metal cationoxygen covalency, <sup>25-27</sup> position of the O 2*p*-band center relative to the Fermi level, <sup>26</sup> and adsorbate free energies.<sup>28</sup> Establishing relationships between electronic properties and OER activity—with distinction between properties of the pristine versus the transformed electrocatalyst surface—is necessary for understanding how to design pre-catalysts that will reconstruct to form highly active

Surface Pourbaix diagrams capture the thermodynamically stable surface(s) as a function of applied potential and electrolyte pH [Fig. 1(b)]. During OER, thermodynamic differences in (bulk) phase stability and adsorbate coverage can lead to changes in metal oxidation state at the surface, in some cases extending to phase changes at greater depth as well.<sup>30, 31</sup> Surface Pourbaix diagrams show that the nominal oxidation state of surface metal cations increases as the driving force for the OER (applied anodic electrochemical potential) increases commensurate with the adsorption of OER intermediates [Fig. 1(b)]. Both experimentally and calculated surface Pourbaix diagrams can be used to predict the possible dissolution of metal cations into the electrolyte. <sup>29, 32,</sup> 33

5

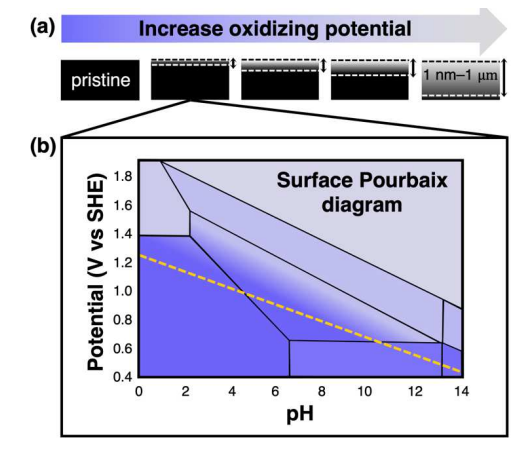


FIG. 1. Electrocatalyst surface restructuring. (a) Illustration of varying scales of electrocatalyst surface transformation in response to an anodic electrochemical potential. (b) General Pourbaix diagram (not computed) for an arbitrary OER electrocatalyst. The dashed yellow line indicates the standard potential for water oxidation.

In this review, we highlight the importance of approaching OER electrocatalysis with an emphasis on surface characterization. We do this through examples of surface transformations of perovskite oxides, spinels, and dichalcogenides, followed by characterization-focused discussion. Our goals for this work are to explain how experimental techniques detect surface transformations, motivating a suite of characterization approaches and in some cases, developing new techniques to probe these dynamic phenomena. Each characterization technique yields area-averaged or volume-averaged information to a varying extent. Understanding 1) the basic mechanism, 2) advantages, 3) limitations, 4) and rational for combining certain characterization techniques, we hope our review will inform how OER electrocatalyst surface transformations can be studied. Ultimately, we urge researchers to further develop structure-transformation relationships to inform the rational design of OER pre-catalysts.

PLEASE CITE THIS ARTICLE AS DOI: 10.1063/5.0139558

## DETECTION OF ELECTROCATALYSTS' DYNAMIC SURFACE CHANGES

Here we present experimental techniques used to detect surface changes on electrocatalysts during the OER, including real-space imaging, spectroscopy with composition/chemical sensitivity, and diffraction-based approaches. We provide the type of information that can be achieved from each technique, advantages, limitations, relevant examples, and tips for pairing complimentary techniques. First, we present electron microscopy techniques including (electrochemical or high-resolution) transmission electron microscopy (TEM, e-TEM, and HRTEM), electron energy loss spectroscopy (EELS), high angular annual dark field (HAADF) imaging, and scanning transmission electron microscopy energy dispersive spectroscopy (STEM EDS). Next, we introduce vibrational techniques including Fourier-Transform Infrared (FTIR) spectroscopy and Raman spectroscopy for probing high surface area electrocatalysts. Core level spectroscopy methods discussed include (ambient pressure) x-ray photoelectron spectroscopy (AP-XPS) and x-ray absorption spectroscopy (XAS), encompassing both x-ray absorption near edge structure (XANES) and extended x-ray fine structure (EXAFS). Lastly, we discuss x-ray diffraction (XRD) based as surface probe techniques including surface x-ray diffraction (SXRD), grazing incidence x-ray diffraction (GI-XRD), crystal truncation rod (CTR) and x-ray reflectivity (XRR).

Visualizing Changes in Real Space Atomic Arrangement by Electron Microscopy Atomic-scale imaging of electrocatalysts during/after electrochemical cycling is perhaps the most intuitive illustration of surface transformations. In situ (electrochemical) and ex situ TEM give insight into the transformation depth, microstructure and morphological changes, and phase transformations of the surface with respect to the structure of the bulk material. TEM passes high energy (50-200 keV) electrons through a thin layer of crystalline solid.<sup>34</sup> If these electrons pass through aligned atomic columns, resolution can be obtained on the order of single atoms, while

PLEASE CITE THIS ARTICLE AS DOI: 10.1063/5.0139558

misaligned planes or disordered atoms appear disordered in the image. With a well prepared sample, many TEM instruments are capable of resolution below 0.1 nm.<sup>35</sup> As this approach operates via transmission of electrons, it contains information about the bulk of the material, though generally the information depth is no more than approximately 20 nm [Fig. 3(a)]. Samples are constrained to maximum thicknesses generally less than 100 nm for TEM, 15 nm for HRTEM,<sup>36</sup> and <50 nm for liquid cell TEM,<sup>37</sup> which limits the catalyst dimensions or requires sample preparation such as cross sectioning using a focused ion beam (FIB). Measuring the edge of materials using TEM—regardless of bulk sample thickness—yields information about the surface.

With recent developments, HRTEM has been used to study electrocatalyst surface changes at an atomic level. To gain information about lattice oxygen, such as ordering, coordination and octahedral tilting, HAADF can be used to increase the contrast between oxygen atoms and heavier metal atoms.<sup>36</sup> The distribution of energy from inelastically scattered electrons to give information about bonding environments and oxidation state can be measured using EELS.<sup>36</sup> For ex situ analyses after OER, EDS can be used to differentiate between dissimilar bulk and surface chemical compositions by changing the spot size of the electron beam.

Electrocatalysts are commonly studied by ex situ TEM before and after electrochemical testing. Ex situ TEM is an excellent choice for many researchers who have access to electron microscopy facilities, but sample preparation becomes an important consideration for samples that require mechanical thinning. The standard cross sectioning method involves depositing a thin metal mask (commonly an amorphous layer of W or Pt) onto the sample surface prior to bombarding the sample with a focused Ga<sup>+</sup> ion beam to cut it into a thin wedge shape.<sup>38</sup> The heavy Ga<sup>+</sup> ions most commonly used for sample thinning can generate heat locally and create an amorphous layer on

PLEASE CITE THIS ARTICLE AS DOI: 10.1063/5.0139558

the surface.<sup>38</sup> Fortunately, strategies such as reducing the beam voltage (to 2 keV) and using low angle of 5° can help mitigate beam damage of the sample.<sup>39</sup> In cases where the electrocatalyst is small enough (particles less than 10 nm in diameter), it may be advantageous to use an in situ electrochemical-TEM technique, or deposit samples directly on a TEM grid that is used as the anode and dried before performing TEM (referred to as pseudo or post in situ).

In situ electrochemical-TEM (e-TEM) is a technique where electrocatalysts can be imaged with simultaneous control of the applied voltage and current, <sup>34, 35</sup> The e-TEM device is a miniature flow cell chip where the electrocatalyst material is applied on small glassy carbon current collector sandwiched between two silicon nitride windows transparent to the electron beam.<sup>35</sup> To maintain structural stability under the stress of the liquid/vacuum interface, commercial silicon nitride windows of liquid TEM cells are typically 20-50 nm thick<sup>40, 41</sup> together with the electrolyte reducing the atomic resolution to several nanometers.<sup>35, 42</sup> Such systems typically employ small volumes of electrolyte (e.g. 2.8 nL), which can limit systems to low rates of reaction (e.g. 10 pA) that avoid gaseous oxygen bubbles.<sup>42</sup> Recent improvements have enabled 0.01-0.1s temporal resolution in in situ e-TEM experiments.34 Interference of the electron beam with the electrochemical signal during e-TEM can be minimized by scanning the electron beam.<sup>20</sup> Improving scanning methods and algorithms for TEM image processing are approaches for achieving better e-TEM resolution.35

While changes in catalyst morphology have been observed using in situ e-TEM, 20 ex situ HRTEM is still needed to provide a more detailed investigation of the electrocatalyst surface. An alternative method for imaging a catalyst in electrolyte is Cryo-TEM, where the catalyst is imaged through vitrified electrolyte. 43 Images with nanometer resolution and sub second temporal resolution are achievable with Cryo-TEM, and image quality is typically better (compared to e-

PLEASE CITE THIS ARTICLE AS DOI: 10.1063/5.0139558

TEM) because undesirable side reactions, evolving oxygen bubbles, and flowing electrolyte are avoided.35 The main disadvantage of Cryo-TEM is that only specific snapshots of surface transformations can be observed once the electrolyte is vitrified and imaged ex situ.

Distinguishing between surface transformations induced by OER—as opposed to the electron beam—is critical in any TEM study of OER electrocatalysts.<sup>44</sup> High energy electron beams can change the sample by knock-on damage, radiolysis, electrostatic charging, and/or emission of secondary electrons. These mechanisms may induce changes to the surface structure<sup>45</sup>—as is the case for knock-on damage—or produce chemical effects, such as formation of reactive species produced by radiolysis<sup>46</sup>. The extent of the electron beam damage to the sample depends on the sample's composition and structure, 45 the dose rate  $(e^-s^{-1}\text{Å}^{-2})$ , 35, 45, 47 the total time the sample is subjected to the electron beam, and the TEM imaging method (i.e. static versus scanning imaging modes).

It is important to assess each sample's susceptibility to beam damage during TEM experiments and adjust the imaging conditions to minimize beam damage. In some cases, it may be possible to rule out certain mechanisms of beam damage.<sup>44</sup> Generally, decreasing the beam voltage, dose rate and/or imaging time are the easiest ways to minimize beam damage. 35,44 If these methods do not suffice to mitigate beam damage, varying rastering speeds or deliberately subsampling by "line-hop" scanning (scanning TEM) and reconstructing TEM images are strategies to reduce the amount of spatial overlap of the beam for each line scan.<sup>47</sup> Best practices for reporting electron microscopy data are to publish movie clips or time-series images to show the timescales of surface stability under the electron beam.

Examples of surface transformations of several material types are illustrated by both ex situ and electrochemical TEM techniques in Fig. 2. The extent of spatial and structural changes ranges

PLEASE CITE THIS ARTICLE AS DOI: 10.1063/5.0139558

from compositional transformation throughout the bulk, amorphous layers formed on the surface, and crystallization.

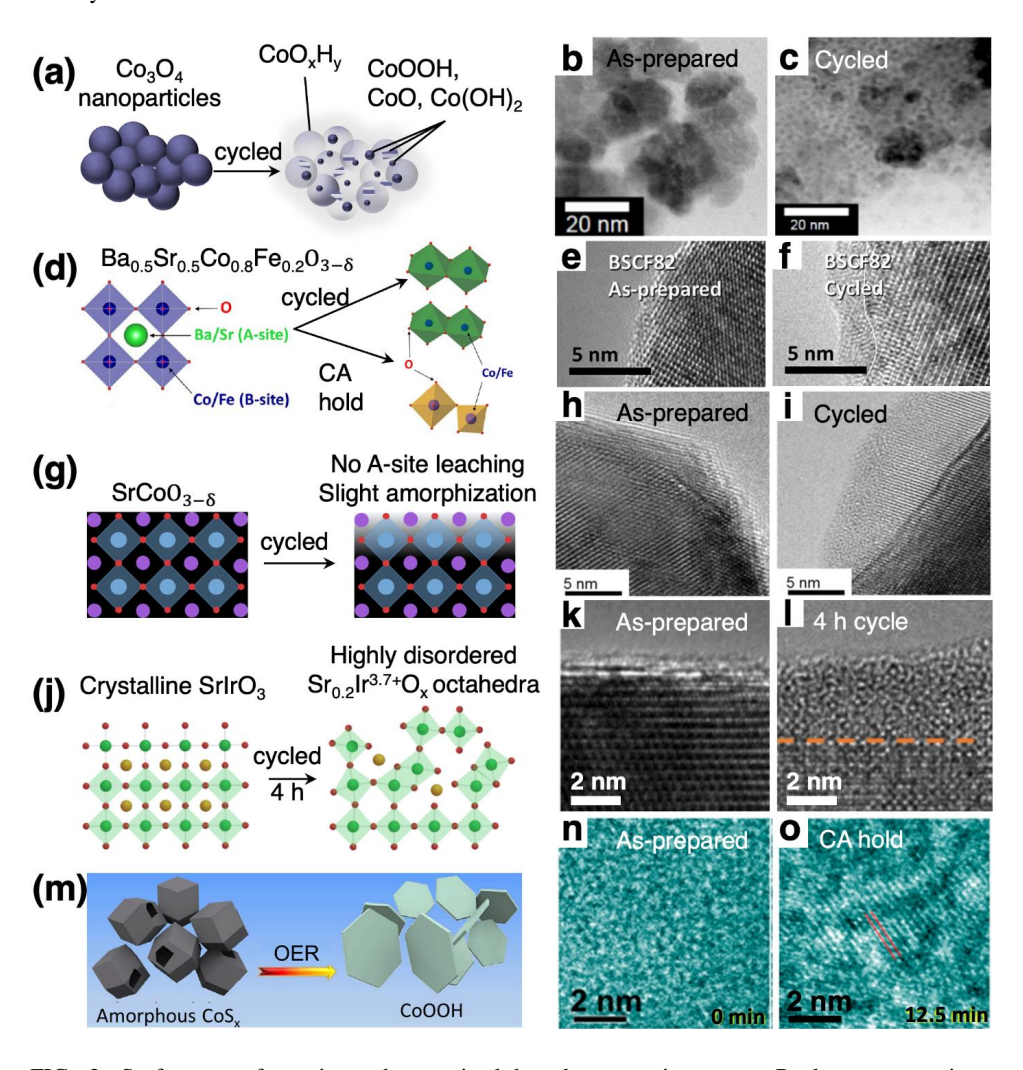


FIG. 2. Surface transformations characterized by electron microscopy. Real space atomic arrangements and rearrangements of several OER electrocatalysts demonstrate a wide range of surface transformation depths. Crystalline Co<sub>3</sub>O<sub>4</sub> spinel (a, b) transforms into an amorphous

PLEASE CITE THIS ARTICLE AS DOI: 10.1063/5.0139558

CoO<sub>x</sub>H<sub>y</sub> matrix with regions of crystalline CoO, CoOOH, and Co(OH)<sub>2</sub> (a, c).<sup>20</sup> The BSCF perovskite surface (d) transforms from a crystalline solid (e) to an amorphous layer (f) as octahedral units rearrange to edge- and corner-sharing coordination. 12, 13 The surface of the crystalline perovskite  $SrCoO_{3-\delta}$  (g, h) becomes slightly amorphous (i) with little Sr leaching from the perovskite. 16 Octahedral units in the SrIrO<sub>3</sub> perovskite become disordered (j) from the crystalline starting material (k), forming a thin amorphous surface layer (l).<sup>21</sup> Initially amorphous CoS<sub>x</sub> dodecahedron (m, n) transform into crystalline CoOOH platelets (o).<sup>22</sup> Panels (a-c) are adapted with permission from ACS nano 13, 10 (2019), Copyright 2019 American Chemical Society. Panels (d-f) are adapted with permission from J. Phys. Chem. 3, 22 (2012). Copyright 2012 American Chemical Society. Panels (h-i) are adapted with permission from J. Phys. Chem. C 122, 15 (2018). Copyright 2018 American Chemical Society. Panels (j-l) adapted with permission from G. Wan, J. et al., Science advances, 7, 2, 2021; licensed under a Creative Commons Attribution (CC-BY-NC) license. Panels (m-o) adapted with permission from ACS nano 12, 12 (2018). Copyright 2018 American Chemical Society.

Heterogeneous transformation of a simple oxide, Co<sub>3</sub>O<sub>4</sub> nanoparticles is shown in Figs. 2(a), 2(b), and 2(c). Ortiz-Peña and colleagues (2019) were the first to study surface transformation during OER using an in situ e-TEM technique. 20 They found that spinel Co<sub>3</sub>O<sub>4</sub> nanoparticles [Figs. 2(a) and 2(b)] transformed to isolated regions of crystalline CoOOH, CoO, and Co(OH)2 embedded in an amorphous CoO<sub>x</sub>H<sub>y</sub> matrix [Figs. 2(a) and 2(c)]. The non-uniform amorphization of the Co<sub>3</sub>O<sub>4</sub> nanoparticles caused an increase in the OER activity after 120 cyclic voltammetry (CV) cycles in 0.1 M KOH.<sup>20</sup> An ex situ TEM study of the Co<sub>3</sub>O<sub>4</sub> nanoparticles before and after a 2 h chronoamperometric (CA) hold at 10 mA cm<sup>-2</sup> confirmed that the amorphization process was irreversible and independent of the electron beam.<sup>20</sup>

PLEASE CITE THIS ARTICLE AS DOI: 10.1063/5.0139558

Several examples of perovskite oxides by ex situ TEM show spatial variation throughout the depth of the surface, resulting in formation of an amorphous surface layer. This amorphous surface layer has been interrogated by EELS, HAADF, and STEM EDS analyses. Ex situ TEM of the BSCF82 showed significant surface amorphization after electrochemical cycling in alkaline media at OER potentials [Fig. 2(f)]. Using EELS, May et al. (2012) determined that Ba and Sr site cations (A-site cations) leached from the surface of BSCF82 [Figs. 2(e) and 2(f)]. Analysis of the EELS spectra indicated that the ~100 nm thick amorphous layer was edge-sharing CoO<sub>6</sub>/FeO<sub>6</sub> octahedra in a spinel structure after 5 CV cycles [Fig. 2(d)]. <sup>12</sup> High angular annual dark field (HAADF) imaging paired with scanning STEM EDS was used to quantify a loss of both A-site cations from the top 10 nm of the sample. 12 A metal (oxy)hydroxide layer consisting of corner- and edge-sharing BO<sub>6</sub> octahedra formed the active OER surface. <sup>13, 29, 48</sup> The BO<sub>6</sub> octahedra (CoO<sub>6</sub> and FeO<sub>6</sub>) were characterized by Raman spectroscopy as discussed in section 2.2. Similarly, ex situ TEM and HRTEM combined with EDS were used to study surface amorphization of the perovskite oxide SrCoO<sub>3-δ</sub> [Figs. 2(g), 2(h) and 2(i)] in alkaline media. <sup>16</sup> Unlike the BSCF82 perovskite,  $SrCoO_{3-\delta}$  showed only slight surface amorphization and no significant A-site Sr leaching based on ex situ HRTEM images [Figs. 2(g), 2(h), and 2(i)]. Although BSCF82 and  $SrCoO_{3-\delta}$  were both cycled in alkaline electrolyte, they exhibit dissimilar surface changes, illustrating composition plays an important role in the nature of the surface transformation during OER. ex situ TEM images of cross-sectioned SrIrO<sub>3</sub> clearly show the pristine [Fig. 2(k)] and amorphous

A study of SrIrO<sub>3</sub> in acidic media by Wan et al. (2021) demonstrated the loss of crystalline structure from OER cycling and linked the lattice oxygen activation to metal dissolution and surface amorphization using ex situ TEM and synchrotron-based surface x-ray techniques. 21 The

This is the author's peer reviewed, accepted manuscript. However, the online version of record will be different from this version once it has been copyedited and typeset PLEASE CITE THIS ARTICLE AS DOI: 10.1063/5.0139558

leached from the single crystal SrIrO<sub>3</sub>(001)<sub>psuedo-cubic</sub> surface during CV cycling due to the presence of oxygen vacancies in the open square-planar network [Figs. 2(g), 2(h), and 2(i)].<sup>21</sup> The rate of oxygen vacancy formation exceeds that of vacancy regeneration from H<sub>2</sub>O leading to collapse of the octahedral units and formation of a ~2.4 nm thick amorphous IrO<sub>x</sub> surface [Figs. 2(j) and 2(l)]. Further discussion of the SrIrO<sub>3</sub> surface is detailed by diffraction and core level studies described in section 2.3. In addition to A-site leaching, the transformed surface of Ir-based double perovskites may be controlled by changing the thermodynamic stability of a substituted Bsite. Chen et al. (2021) tested this concept with the perovskites SrCo<sub>0.5</sub>Ir<sub>0.5</sub>O<sub>3</sub> and SrSc<sub>0.5</sub>Ir<sub>0.5</sub>O<sub>3</sub>, where facilitating partial dissolution of B-site cations from the surface increases the ability of Sr to migrate out of the lattice into the electrolyte to increase the number of Ir sites exposed to the electrolyte. 49 Cobalt leached slightly from SrCo<sub>0.5</sub>Ir<sub>0.5</sub>O<sub>3</sub> while a greater amount of Sc leached from SrSc<sub>0.5</sub>Ir<sub>0.5</sub>O<sub>3</sub> in acidic media, leading to a greater amount of A-site Sr leaching from SrSc<sub>0.5</sub>Ir<sub>0.5</sub>O<sub>3</sub> compared to SrCo<sub>0.5</sub>Ir<sub>0.5</sub>O<sub>3</sub>. Surface-sensitive XAS measurements and simulated O-K edge XANES suggested the transformed surface of SrCo<sub>0.5</sub>Ir<sub>0.5</sub>O<sub>3</sub> was H<sub>2</sub>IrO<sub>3</sub> in a honeycomb structure. 49 Thus, partial leaching of B-site cations control the magnitude of A-site leaching in ABO<sub>3</sub> perovskites and impact the transformation to active OER surfaces.

[Fig. 2(1)] surface before OER and after 4 h of potential cycling, respectively. Sr A-site atoms

In addition to loss of crystalline structure, TEM can also track crystallization processes resultant from the electrochemical environment. Fan et al. (2018) chose a pseudo in situ TEM technique to study amorphous CoS<sub>x</sub> nanoparticles.<sup>22</sup> Ex situ TEM was used to observe initially amorphous  $CoS_x$  [Figs. 2(m) and 2(n)] transform into highly active polycrystalline  $\alpha$  – CoOOH nanoplatelets with displacement of sulfide ligands via reactivity with water and oxygen [Figs. 2(m) and 2(o)]. The final surface consisted of Co(III) oxide or (oxy)hydroxide.<sup>22</sup> HAADF and EDS

PLEASE CITE THIS ARTICLE AS DOI: 10.1063/5.0139558

color map images taken at timed intervals throughout a chronopotentiometry (CP) experiment (at 0.5 mA cm<sup>-2</sup>) showed decreases in Co and S and increases in O atoms accompanying the amorphization process.<sup>22</sup>

Together, these examples illustrate the utility of electron microscopy for directly observing changes in atomic arrangements near at the electrocatalyst surface. Unfortunately, in situ and operando TEM studies are less easily achieved due to complex experimental setups, in situ liquid TEM cells are generally less accessible to many researchers, and ex situ TEM measurements cannot achieve real-time information about surface transformations as a function of voltage or current.<sup>35</sup> Spatially resolved information about the element distribution can be obtained from EDS and EELS, and electronic structure can—to some extent—be determined by the latter. These methods can be complemented by spatially averaged insight into the electronic structure and adsorbed reaction intermediates via coupling with vibrational, core level, and diffraction-based techniques.

## Vibrational Spectroscopic Methods B.

Vibrational spectroscopy techniques provide physiochemical information specific to chemical bond strength, polarization, electrocatalyst lattice symmetry, local defects, short-range ordering, and electrochemical processes at the electrode-electrolyte interface.<sup>50</sup> Due to the wavelengths of visible or infrared probes, data are generally area-averaged on a length scale in the range of microns (for reflectance configurations, Figs. 3(b), 3(c) and 3(d)). The exact information depth depends on the scattering power of the electrocatalyst material which usually extends into the bulk. Experimental configurations can generally accommodate a large range of sample thicknesses, morphologies, and crystallinity.<sup>51</sup>

Fourier transform infrared (FTIR) and Raman spectroscopies are the two most common vibrational spectroscopy methods used to characterize and quantify changes on the electrocatalyst

PLEASE CITE THIS ARTICLE AS DOI: 10.1063/5.0139558

surface [Fig. 3(a)]. Commercially available *in situ* FTIR and Raman cells make these types of experiments among the most accessible to researchers. Both techniques are nondestructive and somewhat modifiable lab-based methods, making them well-suited for custom experimental designs. For example, confocal backscattering Raman probes [Fig. 3(d)] may be modified to interface with FTIR for *operando* spectroelectrochemistry.

Fourier Transform Infrared spectroscopy techniques give information about bending modes and asymmetric vibrations of adsorbate species by measuring changes in molecular dipole moments of hetero-nuclear covalent bonds. Absorption of incident infrared light occurs at frequencies (or wavelengths) that resonate with that of the adsorbed molecule. The transmitted infrared light is converted by a Fourier transform spectrometer into an absorbance for each wavelength (sensitive to the masses of bonded atoms or molecules) to create the spectrum. To reduce interfering signal from the aqueous electrolyte, a thin 1-100 µm electrolyte layer separates the electrocatalyst from a hemispherical IR-transparent window typically made from CaF<sub>2</sub>, Si, or ZnSe [Fig. 3(b)].<sup>8</sup>

An internal ATR-FTIR configuration [Fig. 3(c)] is a good choice to minimize strong signal from the aqueous electrolyte. In this technique, incident light travels through an grooved, IR-transparent ATR crystal (typically Si, Ge, ZnS, ZnSe, diamond/ZnSe) with the bottom face cut at specific angles and the top face coated with a thin layer of electrocatalyst material.<sup>8</sup> Reflections of incident IR irradiation produce multiple evanescent waves that attenuate ~5-10 nm into the electrocatalyst-electrolyte interfacial region [Fig. 3(c)].<sup>52</sup> This configuration dramatically reduces the strong IR absorption bands from water, provides more surface sensitive information, and increases the signal five-fold compared to the external reflection mode.<sup>52</sup>

PLEASE CITE THIS ARTICLE AS DOI: 10.1063/5.0139558

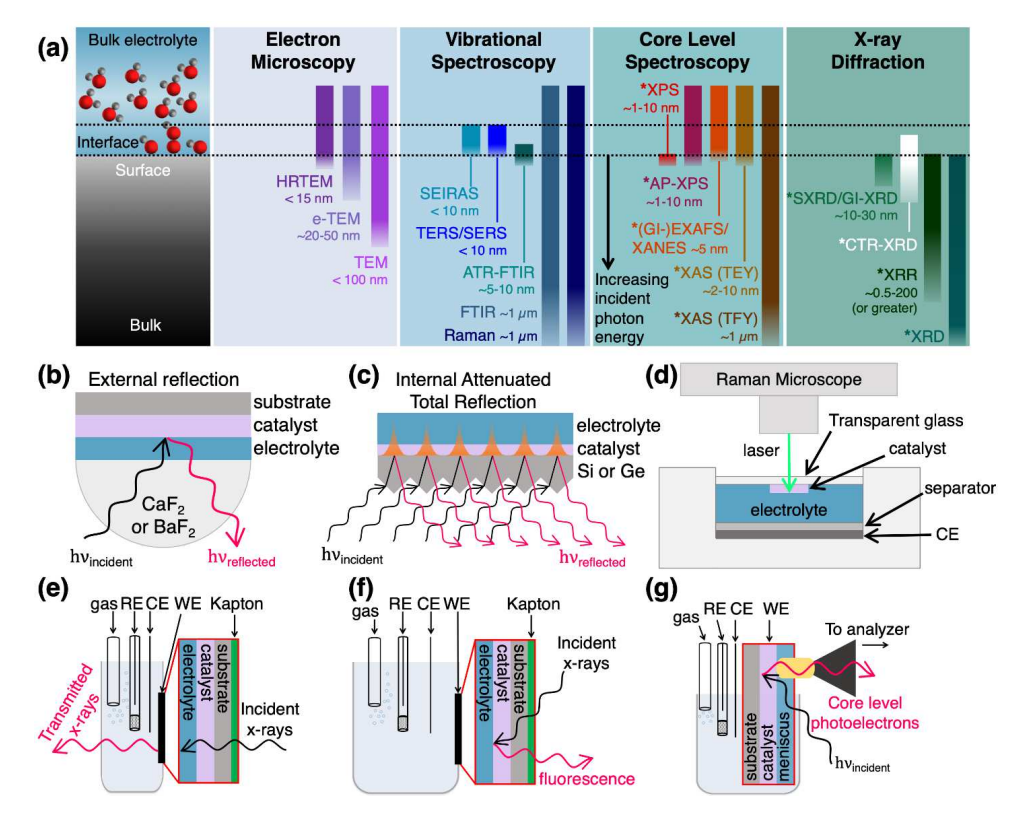


FIG. 3. Information depths for several characterization techniques with respect to the electrocatalyst material (a), electrocatalysts/electrolyte interface, and the bulk electrolyte (scale bars are approximate to show how techniques compare qualitatively). The information depth from techniques marked with asterisks is dependent on incident photon energy or x-ray energy, with higher energies generally probing deeper into the surface. In situ or operando (b) external reflection Fourier-Transform Infrared (FTIR) spectroscopy and (c) attenuated total reflection FTIR (ATR-FTIR). Confocal Raman spectroscopy (d) is based on 180° backscattering. Examples of electrochemical cells used for synchrotron-based transmission XAS (e), fluorescence XAS, (f), and ambient-pressure XPS (g). Panel (e) adapted with permission from J. Am. Chem. Soc. 141, 4

## This is the author's peer reviewed, accepted manuscript. However, the online version of record will be different from this version once it has been copyedited and typeset. PLEASE CITE THIS ARTICLE AS DOI: 10.1063/5.0139558

(2019). Copyright 2019 American Chemical Society. Panel (g) adapted with permission from Top. Catal. 61, 20 (2018). Copyright 2019 Springer Nature.

Raman spectroscopy probes symmetric vibrational modes of adsorbate species by measuring the difference in frequency between incident and scattered visible light resulting from the polarizability of homo-nuclear bonds. Inelastically scattered light, known as Raman scattering, occurs when incident light imparts or gains energy when it interacts with an adsorbed molecule.<sup>53</sup> Primarily, Stokes lines are measured from energy imparted to the adsorbate from the incident irradiation.<sup>8</sup> Monochromatic visible light is used for Raman spectroscopy, so glass cells and aqueous solutions pose no issues.<sup>8</sup> For example, the surface amorphization of BSCF82 was confirmed using Raman spectroscopy, as a notable band at 675 cm<sup>-1</sup>, assigned to the vibrational mode of O in CoO<sub>6</sub> and FeO<sub>6</sub> octahedra, broadened and decreased in intensity with continued CV cycling above the onset of OER.<sup>12</sup>

Further enhancement of signal select to the electrocatalyst surface can be obtained by their support on a plasmonic metal (Au, Ag, or Cu, and less commonly Pt, Pd, Rh, or Ru) which localizes the electric field. Such techniques include surface-enhanced infrared absorption spectroscopy (SEIRAS), surface enhanced Raman spectroscopy (SERS), and tip-enhanced Raman spectroscopy (TERS). SERS increases the surface sensitivity for detection of monolayers of surface adsorbates using localized plasmonic resonance, and is more sensitive to light atoms at the electrocatalyst-electrolyte interface compared to x-ray techniques. In situ SERS was used to study surface transformation of Au-supported Co<sub>3</sub>O<sub>4</sub> to CoO(OH) under OER conditions, providing additional evidence that CoO(OH) may be a common active surface during OER for multiple Co-derived starting materials. Efforts to expand to non-noble metal substrates with acceptable signal enhancement factors will make SERS more broadly applicable. TERS can achieve nanometer

PLEASE CITE THIS ARTICLE AS DOI: 10.1063/5.0139558

spatial resolution by integrating a Raman microscope with and atomic force microscope (AFM) or a scanning tunneling microscope (STM) to magnify the signal at the sharp tip.<sup>50</sup> Recently-developed TERS and single-molecule SERS are promising techniques for revealing site-specific phenomena instead of an ensemble response from many atoms, though *in situ* electrochemical-TERS is still being developed.<sup>57</sup>

Depending on the kinetics of a specific electrocatalyst material, the stretching and bending modes of OER intermediates—including OH<sub>ads</sub>, O<sub>ads</sub>, and OOH<sub>ads</sub>—adsorbed to an electrocatalyst surface may be present as absorbance bands a SEIRAS the spectra. In addition, the high probability of infrared absorption, compared to the rare event of Raman scattering, yields greater SEIRAS signal that can then be collected quickly to achieve high temporal resolution—as low as picosecond time-resolution—giving valuable information about rapid surface changes including double layer charging and vibrational changes of surface adsorbates.<sup>54, 58</sup>

Both FTIR and Raman have been used extensively to probe changes in OER electrocatalysts during electrochemical cycling. For example, *in situ* FTIR was used to monitor the conversion from pristine chalcogenides to oxides during OER. Spectra of initially amorphous CoS<sub>x</sub> during a CP experiment (1000 s at 1 mA cm<sup>-2</sup>) was used to observe crystallization to an α – CoOOH phase [Fig. 4(a)].<sup>22</sup> The FTIR bands at 3350 cm<sup>-1</sup> and 1630 cm<sup>-1</sup>—assigned to the stretching and bending vibrational modes of hydrogen-bonded OH<sub>ads</sub>, respectively—indicated transformation after the first 400s shown in the yellow spectrum in Fig. 4(a). The spectral intensity of the band located at 892 cm<sup>-1</sup> increased and reached a steady state after 1000 s shown in the blue spectrum in Fig. 4(a), which is ascribed to the bending mode of structural O–H on the a Co oxide or Co (oxy)hydroxide surface.<sup>22</sup> There was no change in the spectrum upon removal of the applied

PLEASE CITE THIS ARTICLE AS DOI: 10.1063/5.0139558

current shown in the purple spectrum in Fig. 4(a) indicating that the surface changes were irreversible. (b) (a) Removal of bias NiOOH 1000 s

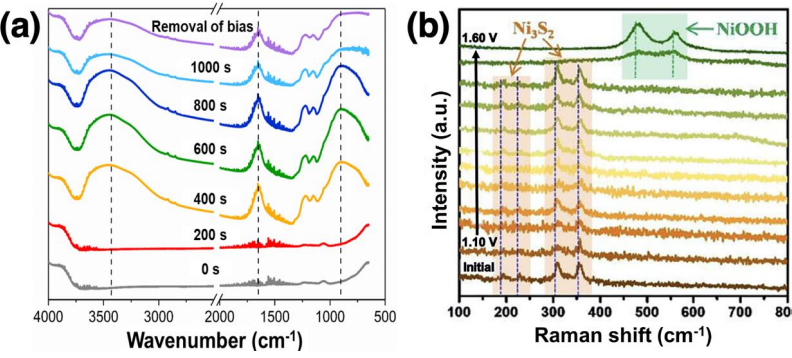


FIG. 4. In situ vibrational spectroscopy techniques. Panel (a) shows in situ FTIR of CoSx with 1 mA anodic current in 1 M KOH, 22 (b) in situ Raman of ternary Fe-Co-Ni dichalcogenide nanowires,<sup>59</sup> Panel (a) adapted with permission from ACS nano 12, 12 (2018). Copyright 2018 American Chemical Society. Panel (b) adapted from J. Energy Chem. 55 (2021). Copyright 2021 Elsevier B.V..

Similarly, in situ Raman spectroscopy has been used to observe surface oxidation with concurrent removal of S atoms of dichalcogenides and spinels OER electrocatalysts in alkaline media (KOH). For a high surface area crystalline FeCoNi-S dichalcogenide (FCND) nanorod array [Fig. 4(b)],<sup>59</sup> the onset of OER occurred around 1.4 V versus reversible hydrogen electrode (RHE) (with bands at 211 cm<sup>-1</sup>, 250 cm<sup>-1</sup>, 327 cm<sup>-1</sup>, and 372 cm<sup>-1</sup> ascribed to NiS<sub>2</sub>), but no shifts in the Raman peaks were observed until the applied potential reached 1.5 V, where two bands attributed to NiOOH at 484 cm<sup>-1</sup> and 558 cm<sup>-1</sup> appeared.<sup>59</sup> For the sulfur spinel, Co<sub>9</sub>S<sub>8</sub>, [Fig. 3(d)],<sup>60</sup> oxidation to Co<sub>3</sub>O<sub>4</sub> quickly occurred before a complete conversion to a CoOOH surface layer at potentials above 1.4 V versus RHE.<sup>60</sup> Increased Raman peak widths observed after reversal of the applied potential indicated that the crystalline-to-amorphous transition was semi-reversible. <sup>60</sup>

PLEASE CITE THIS ARTICLE AS DOI: 10.1063/5.0139558

The processes of a material surface transforming from crystalline to amorphous can be tracked via the broadening and/or shifting of fingerprints as a function of applied potential or current. New structural phases or changes in site occupation may present themselves in vibration spectra as new bands, intensity changes of existing bands, band broadening, or shifting bands.<sup>50</sup> To quantitatively assess electrocatalyst materials, the full width at half maximum (FWHM) gives information about the homogeneity of chemical bonding.<sup>51</sup> Peak positions of FTIR and Raman spectra are commonly used to qualitatively assign stretching and bending modes of specific species. Unfortunately there are no universally accepted IR and Raman standards for short-lived reaction intermediates or metastable phases, which can sometimes lead to ambiguous peak assignments for these species.<sup>52</sup> Moreover, cross sections of adsorbates sometimes overlap with other bands which may limit the amount of information that can be extracted from vibrational spectroscopy studies. 61 Therefore it is recommended to pair vibrational spectroscopy experiments with other surface-sensitive techniques. In the next section, core level spectroscopy techniques are introduced to give insight into the electronic structure of the surface such as oxidation state changes and binding affinities of reaction intermediates.

## Core level spectroscopic characterization techniques

In contrast to vibrational spectroscopies that give insight into the strength of interatomic bonds, core level techniques provide element-specific information about local electronic structure, local bonding environment, and average oxidation state. 52,62 Core level techniques such as XAS can probe the bulk in transmission mode [Fig. 3(e)] and in fluorescence mode as well [Fig. 3(f)]. Measurement of ejected photoelectrons directly in AP-XPS [Fig. 3(g)] or indirectly as a grounding current in electron-yield mode XAS provides increased surface sensitivity.

X-ray photoelectron spectroscopy can illustrate elementally specific changes inherent to the top 1-10 nm of the surface. Incident photons inelastically scatter core level electrons



PLEASE CITE THIS ARTICLE AS DOI: 10.1063/5.0139558

(photoelectrons) from atoms and elastically scatter secondary electrons (Auger electrons) via the photoelectric effect. An electron analyzer quantifies the scattered electrons as a function of their kinetic energy, which is converted to their respective binding energies. Binding energies are characteristic to elemental identity, and small shifts in the binding energy arise from the chemical shifts, or the local chemical environment of each atom. The information depth of (AP-)XPS depends on experiment parameters such as the energy of the incident photons  $(h\nu)$  or x-rays, the kinetic energy of ejected photoelectrons, and the angle of incidence and emission, as well as the type of electrocatalyst material [Fig. 3(a)]. X-ray energies are categorized into three regimes: "hard" ( $h\nu > 5$  keV), "tender" ( $h\nu \sim 2-5$  keV), and "soft" ( $h\nu < 2$  keV). Surface sensitive techniques employ soft x-rays that probe the top few nanometers of the sample surface due to the short inelastic mean free path of ejected core level photoelectrons. Soft and tender x-rays are used to probe catalyst surfaces through gases for in situ techniques and tender and hard x-rays have sufficient energy to penetrate liquid electrolytes during operando x-ray experiments. Depth profiling can be achieved by varying the incident photon energy or by changing the angle of the incident photons.<sup>63</sup> These factors, together with the beam spot size, control the probed volume.

X-ray absorption spectroscopy encompasses both XANES and EXAFS. XANES covers energies from ~200 eV below the absorption edge to ~50 eV above the absorption edge, while EXAFS extends to higher energies above the adsorption edge. <sup>64, 65</sup> XANES is primarily used to determine oxidation state, orbital spin and splitting, and 3d transition metal-oxygen covalency by measuring the position and shape of the absorption edge. The absorption edge arises from the excitation of photoelectrons to unoccupied states. In transmission mode [Fig. 3(e)], the x-ray signal attenuates as a function of sample thickness, so the sample (and the cell, if operando) must sufficiently thin (~100 nm). In fluorescence yield mode, the emitted secondary x-rays are detected

PLEASE CITE THIS ARTICLE AS DOI: 10.1063/5.0139558

while in electron yield mode relaxation of core-holes cause Auger electron emission and total electron emission is detected. Surface sensitivity of XANES is greater when probing total electron yield (TEY) XANES, which has an information depth limited by the escape depth of electrons from the surface (typically ~2-10 nm) compared to total fluorescence yield mode (TFY, information depth ~microns) [Fig. 3(a)].66 EXAFS, on the other hand, probes the XAS spectrum above the absorption edge and is sensitive to bond lengths and local structure. When the incident x-ray beam is position at a grazing incidence relative to the sample surface, more surface-sensitive information can be obtained [Fig. 3(a)]. To extract quantitative electronic and chemical structure information from XAS spectra, it is critical to choose well-defined reference materials (with welldefined crystal structure and oxidation state) and perform related analysis.<sup>64</sup>

As with other techniques, slight changes in the electrocatalyst surface may arise from experiment conditions (i.e., OER) or from x-ray beam damage during core level spectroscopy experiments. The possibility of beam damage can be assessed by systematic measurements of multiple spots on the sample and monitoring changes in the spectra as a function of incident photon energy, incident photon flux, spot size, and rastering speed (if a scanning method is used). Other ways to improve the study quality are to characterize multiple spots to ensure a consistent response across the sample, use shorter or discreet measurements (collecting several spectra and averaging them), and switch the beam on and off at varied beam intensities while continuously collecting spectra.

Examples of in situ and ex situ core level spectroscopy and x-ray diffraction techniques are presented for thin film electrocatalysts in Fig. 5. Sensitivity to controlled surface terminations on LaNiO<sub>3</sub> perovskite thin films are highlighted in the work of Baeumer et al. (2021) [Fig. 5(a)].<sup>67</sup> Here, XPS is capable of distinguishing differences in termination of complex oxides, for instance

This is the author's peer reviewed, accepted manuscript. However, the online version of record will be different from this version once it has been copyedited and typeset PLEASE CITE THIS ARTICLE AS DOI: 10.1063/5.0139558

The Ni 3p XPS before and after OER [Fig. 5(a)] show a high binding energy shoulder on the LNO-Ni that is not present in the LNO-La spectrum, supporting the conclusion that a hexagonal NiO<sub>x</sub> phase forms on the top unit cell of the LNO-Ni thin film at highly oxidizing potentials. <sup>67</sup> The LNO-

between NiO<sub>x</sub> versus LaO<sub>x</sub>-terminated LaNiO<sub>3</sub> (abbreviated LNO-Ni and LNO-La, respectively).

Ni films show a higher activity compared to LNO-La films, and surface terminations play an

important role in both surface transformation processes and subsequent OER activity, a finding

that was generally true for LaO and FeO<sub>2</sub>-terminated LaFeO<sub>3</sub> perovskites. <sup>67, 68</sup>

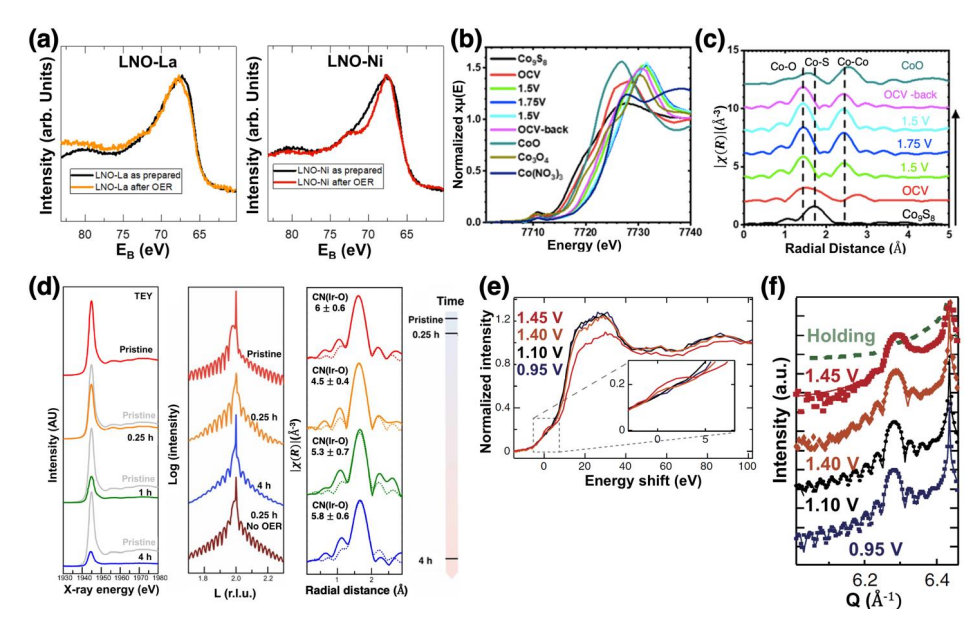


FIG. 5. Core level and x-ray diffraction-based characterization techniques. (a) Ni 3p core level of La- and Ni-terminated LaNiO<sub>3</sub> thin films is characterized by XPS. <sup>67</sup> (b) in situ XANES and (c) EXAFS of Co<sub>9</sub>S<sub>8</sub> thin films measured in fluorescence mode. <sup>60</sup> (d) SrIrO<sub>3</sub> thin films characterized by TEY XANES of Sr L3-edge (d, left), CTR (d, center), and grazing incidence GI-EXAFS of Ir L3-edge (d, right).21 (e) SrRuO3 thin film characterized by Ru K-edge XANES as a function of

PLEASE CITE THIS ARTICLE AS DOI: 10.1063/5.0139558

applied potential.<sup>23</sup> (f) SrRuO<sub>3</sub>(001) thin film characterized by specular rod scans XRD as a function of applied potential.<sup>23</sup> Panel (a) adapted with permission from Nat. Mater. 20, 5 (2021). Copyright 2021 Springer Nature. Panels (b) and (c) reproduced with permission from M. Wang, et al. JACS Au, 1, 12, 2021; licensed under a Creative Commons Attribution (CC BY-NC-ND) license. Panel (d) adapted with permission from G. Wan, J. et al., Science advances, 7, 2, 2021; licensed under a Creative Commons Attribution (CC-BY-NC) license. Panels (e) and (f) adapted with permission from Nat. Commun. 5, 1 (2014). Copyright 2014 Springer Nature.

Oxidation state changes can also be obtained using operando XANES. For example, in-situ XAS was used to identify the active sites of a Co<sub>2</sub>S<sub>8</sub> OER electrocatalyst.<sup>60</sup> The Co K-edge XAS was measured in florescence mode as the applied potential was first increased to 1.75 V and then decreased back to the open circuit potential [Fig. 4(b)]. The shift of XANES spectra suggests the changes of Co oxidation state, confirming the oxidation of Co<sub>9</sub>S<sub>8</sub>. A Fourier transform of the EXAFS region [Fig. 4(c)] shows the Co-S peak diminished shortly after introduction to the alkaline electrolyte. With increasing anodic potential above the onset of OER, the Co-O and Co-Co peaks shift, and upon reversal of the potential bias below the OER onset, the peaks remain at the same radial distances [Fig. 3(c)]. These data indicate an irreversible oxidation of the Co<sub>9</sub>S<sub>8</sub> to a lowcrystalline Co<sub>x</sub>O<sub>y</sub>(OH)<sub>z</sub> material accompanied by irreversible oxidation of Co cations.<sup>60</sup>

Comparison between the XANES intensities from TEY [Fig. 5(d, left)] and TFY revealed that the loss of Sr cations from the surface of SrIrO<sub>3</sub> was greater than loss from the bulk after OER.<sup>21</sup> The Ir L<sub>3</sub>-edge GI-EXAFS [Fig. 5(d, right)] shows an initial decrease in coordination number of Ir-O at 0.25 h of cyclic voltammetry in acidic media (CV between 1.05 and 1.75 V versus RHE), which may be due to evolution of lattice oxygen.<sup>21</sup> After 4 h of cyclic voltammetry, continued Sr<sup>2+</sup> dissolution causes Ir to reoxidize into octahedral geometry with mixed 3+/4+

## PLEASE CITE THIS ARTICLE AS DOI: 10.1063/5.0139558

This is the author's peer reviewed, accepted manuscript. However, the online version of record will be different from this version once it has been copyedited and typeset.

valence [Fig. 5(d, right)].  $^{21}$  This finding was corroborated by DFT calculations, wherein  $Ir^{3+}$  atoms preferentially form in a square planar structure with concurrent  $Sr^{2+}$  diffusion from the film surface.  $^{21}$  This work suggests that activation of lattice oxygen occurs as a result of  $Sr^{2+}$  dissolution.  $^{5,\,21,\,26}$ 

Ru K-edge XANES [Fig. 5(e)] was performed to measure shifts in the Ru valence state of a SrRuO<sub>3</sub> perovskite thin film in acidic media.<sup>23</sup> A large shift in the pre-edge peak [Fig. 5(e), inset] shows that at 1.45 V versus RHE the average oxidation state of Ru increases above 4+.<sup>23</sup> Dissolution from polycrystalline SrRuO<sub>3</sub> at Ru valence states above 4+ also occurred in acidic media (0.1 M HClO<sub>4</sub>), but completely stable oxides were inactive toward OER, so the target Ru electrocatalyst should exhibit a balance between stability and activity of Ru-based oxides with an optimum dissolution rate.<sup>69</sup>

Core level spectroscopy techniques can provide detailed information about area-averaged changes in electronic structure in both *in situ* and *ex situ* conditions. Modification of the energy and angle of incident photons allows variable information depths. Next, we turn to x-ray diffraction methods to highlight how structural changes can be detected.

## D. X-ray diffraction characterization techniques

Diffraction-based techniques provide information on the long-range order (or lack thereof) in crystalline solids and their surfaces. The large penetration depth of hard x-rays (microns) results in characterization of the bulk, generally yielding volume-averaged information. However, surface sensitivity can be achieved by either subtracting well-defined substrate diffraction signals (e.g., single crystal) or positioning the incident x-ray beam and sample at a grazing angle relative to each other as is done in SXRD or grazing GI-XRD. XRR, a technique sensitive to depth-dependent material profiles, complements XRD, which provides information about only the crystalline portion of the sample. The thickness of an amorphous surface layer formed on an initially

PLEASE CITE THIS ARTICLE AS DOI: 10.1063/5.0139558

crystalline surface during the OER can be determined by comparing XRR and XRD diffraction patterns, which was implemented by Wan et al. (2021) to calculate the thickness of an amorphous surface layer atop a SrIrO<sub>3</sub> thin film as function of time during CV cycling.<sup>21</sup>

Another diffraction-based technique is the study of crystal truncation rod (CTR). The diffraction from electrocatalyst materials (e.g., thin films) on the surface of the well-defined single crystal substrates is markedly different from bulk electrocatalysts (e.g., powders) because certain surface orientation of the former is truncated while the latter has isotropic orientations of surfaces in average. The intensity of scattered x-rays is normal to the electrocatalyst surface, with an inplane spacing described by interatomic distances that satisfy Bragg's Law. 70 The periodicallyspaced scattering intensities are called crystal truncation rods. The main advantage of CTR are that surface species as thin as monolayer coverages of adsorbates can be detected. 70 The main limitation arises from the use of restricted reciprocal space that is built upon the substrate lattice. As the reciprocal lattice vector, **Q**, is inversely proportional to the x-ray wavelength, decreasing the x-ray wavelength by increasing the x-ray energy is a way to compact the reciprocal space.<sup>70</sup>

Wan and colleagues used XRR, XRD, and CTR to characterize the surface transformation of SrIrO<sub>3</sub> during potential cycling.<sup>21</sup> The distinctive loss in magnitude of oscillation in the log of the intensity of the CTR pattern from approximately 1.7 reciprocal lattice units (r.l.u.) to 1.9 r.l.u. is indicative of surface amorphization during potential cycling (1.05 V to 1.75 V versus RHE) with a noticeable decrease in the magnitude of oscillations after 4 h of cycling shown in the blue trace in Fig. 5(d, center).<sup>21</sup> When the SrIrO<sub>3</sub> was cycled below the OER onset from 0.8 V to 1.0 V versus RHE, the CTR trace showed no large decrease in the intensity from 1.7 r.l.u. to 1.9 r.l.u, demonstrating that amorphization occurs at higher oxidative potentials than the onset of the OER. 21

PLEASE CITE THIS ARTICLE AS DOI: 10.1063/5.0139558

The relationship between activity and crystallographic orientation using single-crystal SrRuO<sub>3</sub> thin films for (001), (110), and (111) orientations in alkaline media was also studied by CTR.<sup>23</sup> Surface roughness of SrRuO<sub>3</sub>(001) [Fig. 5(f)] was measured by in situ specular rod scans from scattering normal to the film surface.<sup>23</sup> The gradual loss of Keissig fringes between reciprocal lattice vector 6 Å-1 to 6.2 Å-1 [Fig. 5(f)] indicate increased surface roughness with increasing applied potential, and eventually after 30 min at 1.45 V versus RHE (in 0.1 M KOH) the SrRuO<sub>3</sub> dissolved completely Fig. 5(f), labelled green 'Holding' trace.<sup>23</sup>

X-ray beam damage during XRD studies can be assessed and mitigated generally by the same strategies listed in section 2C. In particular, it is recommended to use high energy X-ray in XRD studies for reducing the generation of reactive radicals that could induce damages to the electrocatalyst materials and shortening the time of measurements due to the compacted reciprocal space. Addressing the extent of beam damage by hard x-rays during XRD, XRR, and CTR measurements is necessary to correctly attributing structural changes to OER.

## IV. OUTLOOK ON OER ELECTROCATALYST SURFACE TRANSFORMATIONS

Highly oxidizing potentials required to drive the OER often result in surface changes of electrocatalysts, in many cases impacting the activity and stability of the electrocatalyst material. We see a marked shift away from the assumption that electrocatalyst surfaces remain unchanged from their pristine state, with surface transformations being reported for many different types of OER electrocatalysts. Understanding the modes of surface transformations may allow researchers to find commonalities, develop descriptors for pre-catalyst stability, and improve theory.

## Theory and trends for electrocatalyst surface transformations A.

Some of the most common modes of surface transformations discussed in recent literature include dissolution (sometimes followed by redeposition) of metal cations, chemical reaction, atom migration, anion exchange, oxidation, and vacancy formation/refilling. 71, 72 With the range

PLEASE CITE THIS ARTICLE AS DOI: 10.1063/5.0139558

of surface transformations observed throughout the literature, the operational stability of OER electrocatalysts varies widely depending on the starting material (referred to as the pre-catalyst). The specific mode of surface transformation may be controllable by synthesis or processing conditions of the pre-catalyst. Strategies to impact surface transformation include, metal element doping, surface functionalization, defect conformation, interface engineering, nonmetallic element modulation, and surface etching.<sup>73</sup>

The nature and extent of transformation depends on the synthesis and processing conditions used to make the pristine pre-catalyst material, the electrolyte, and the electrochemical technique. As a result of the myriad of unique experimental variables, many reports of surface transformations in the literature are not directly comparable. However, recent reviews by Gao et al. (2021) and Liu et al. (2021) tabulated materials of pre-catalysts, experimental conditions, and the reported reconstructed species, illuminating commonalities for pre-catalyst restructuring.<sup>74, 75</sup> A large number of the Fe-, Co-, and Ni-based materials listed were found to transform to oxyhydroxide surfaces after OER.<sup>75</sup> Among Co-based materials, Co (oxy)hydroxide has been reported as the reconstructed active surface for Co<sub>3</sub>O<sub>4</sub> nanoparticles, <sup>20</sup> P-substituted CoSe<sub>2</sub>, <sup>76</sup> CoAl<sub>2</sub>O<sub>4</sub> spinel, <sup>77</sup> BSCF82, 78 and amorphous CoS<sub>x</sub> starting materials. 22, 74 Understanding trends of surface transformations is necessary for developing surface transformation descriptors.

Descriptors are electronic or structural material properties that scale with catalytic performance, often "semi-universal", or applied to specific material classes. For example, Sun et al. (2020) found that covalency of neighboring octahedral and tetrahedral units in spinel oxides is a way to tune the exposure of metal cations on the surface and control OER activity.<sup>27</sup> A few semiuniversal electronic descriptors for perovskite oxides include metal-oxygen covalency, eg orbital occupancy, hybridization of metal 3d and oxygen 2p bands.<sup>48</sup> Descriptors may also be categorized



PLEASE CITE THIS ARTICLE AS DOI: 10.1063/5.0139558

as structural, such as coordination number, surface density of undercoordinated metal cations, or preferential adsorption on bimetallic/multi-metallic electrocatalysts. 79 However, it has not been established if electronic and structural descriptors based on pristine/pre-catalyst materials accurately reflect the catalytic performance after a surface transformation occurs.

Two descriptors have recently been proposed to benchmark the stability of electrocatalysts: the Stability number (S-number) and Stability Level. The S-number, developed by Geiger et al. (2018), is defined the ratio of evolved oxygen to dissolved metal cations.<sup>5</sup> The S-number was used to describe the stability of crystalline, perovskite-type, and amorphous Ir-based electrocatalysts, capturing the materials' stable lifetime at a given current density. 5 The S-number is considered a universal descriptor and is independent of loading, surface area, and involved active sites.<sup>5</sup> Samira et al<sup>80</sup> used the S-number to characterize the stability of mixed-metal oxides  $(A_{n+1}B_nO_{3n+1}, A = La,$ Sr, Ca, B = Mn, Fe, Co, Ni) in alkaline electrolyte, ascribing low S-numbers to high cation dissolution arising from structural instability as lattice oxygen participates in OER. They found that the restructuring of mixed metal oxides depends on the composition of A-site cations, strain induced by A-site doping, oxide crystal phase, and electrochemical reducibility. 80 The mixed metal oxides form a transition metal oxyhydroxide layer atop a core of original material while A-site cations dissolve into the electrolyte, similar to the behavior observed for perovskites BSCF82 and SrIrO<sub>3</sub>. <sup>12, 21, 80</sup> The perovskite Stability Level developed by Zhao et al. (2021) is a semi-universal descriptor used to rank perovskites by their current density as a function of stability. <sup>29</sup> The Stability Level accounts for different types of perovskite surface transformation mechanisms including cation leaching, reconstruction, and lattice oxygen vacancy/filling. Observed surface changes based on inductively coupled mass spectrometry (ICP-MS), TEM, and XAS as well as the position of the O p-band center relative to the Fermi level are used to rank each perovskite by stability from

PLEASE CITE THIS ARTICLE AS DOI: 10.1063/5.0139558

S-0 (least stable) to S-4 (most stable) to guide researchers looking to develop high performance perovskite electrocatalysts.<sup>29</sup> ICP-MS is an analytical tool that can be used to quantitatively track the dissolution rates of the mixed metal oxides including the dissolution of metal cations. Based on a literature survey of perovskite surface transformations, the OER activity is maximized at S-2, which is defined as "slight surface changes during OER, usually from a new layer on the perovskite and change in octahedral coordination of the B-site," which agrees with the trend that perovskites generally increase in activity with decrease in stability. 81 This may be understood as a shift in the OER mechanism, where activating lattice oxygens form oxygen vacancies and decrease surface stability compared to an adsorbate evolution mechanism.<sup>81</sup>

There are currently no universal periodic trends for 3d transition metals (or other element groups on the periodic table) or specific material structures that holistically describe surface transformation processes. Computational studies help fill the gap in understanding by the ability to process large numbers of candidate pre-catalysts and find trends in likely surface transformations. One of the most important aspects of developing robust computational models is starting with a good understanding the of the pre-catalyst surface. Information about the pristine material surface is a critical requirement for DFT modeling to choose the appropriate model structure, or the exposed surface facet and setting the simulation parameters.<sup>75</sup> For this reason, single crystal thin films are ideal materials to start with because of their relative simplicity of morphology and low surface roughness. However, DFT calculations based on a pristine, preelectrocatalyst surface may not reflect the material's catalytic behavior following a surface transformation, illustrating the importance of probing active surface configurations with in situ or operando techniques. Other popular computational tools including molecular dynamics (or reactive force field molecular dynamics), kinetic Monte Carlo simulations (kMC), and state space

PLEASE CITE THIS ARTICLE AS DOI: 10.1063/5.0139558

modeling (SSM) add insight on electrocatalyst surface transformations.<sup>71</sup> Ideally, experimental researchers work iteratively with collaborators doing computational studies to arrive on the most accurate explanation of surface transformation.

Research on electrocatalyst surface transformations is transitioning toward a deeper understanding of underlying transformation mechanisms at play. It is possible that surface transformations may be too broad to be classified by universal descriptors and are best described in a semi-universal manner by material class, processing conditions, electrochemical operating conditions, or another experimental variable. Nevertheless, if such trends exist, then it may be possible to design pre-catalyst materials that undergo a desired transformation pathway toward an optimized active material. Next, we provide an outlook on advancing the design of pre-catalyst materials.

В. The future of electrocatalyst surface transformations: Achieving optimized pre-

Information about surface transformations can be used to understand OER mechanisms, uncover the location of active sites on the transformed surface, and continue to inform the rational design of OER pre-catalysts. We envision that future research in heterogeneous electrocatalysis will employ this pre-catalyst approach to synthesize an appropriate starting pre-catalyst that will undergo an optimized surface transformation process to yield a highly active surface. This knowledge, assuming the transformed surface reaches a new metastable state (or terminal composition), will improve computational models. Currently, there are few studies that predict the terminal composition or magnitude of surface restructuring. We look to excellent examples from ORR literature that uncover the relationship between pristine and terminal electrocatalyst materials and aided computational studies of ORR electrocatalysts. 82, 83 Similar studies in the realm of OER

PLEASE CITE THIS ARTICLE AS DOI: 10.1063/5.0139558

electrocatalysts will provide information to computational researchers for more accurate prediction of highly active and stable OER electrocatalysts.

Understanding surface transformations is the first step to designing pre-catalysts that transform to optimal OER active phases. A few strategies have been proposed in the literature regarding pre-catalyst design strategies. Liu et al. (2021) suggest that starting with amorphous precatalysts may lower the activation process.<sup>72</sup> As many of the transformed surfaces tend to be an hydroxide or oxyhydroxide surface layer, starting with a hydroxide material may facilitate the transition toward the oxyhydroxide surface. The extent of transformation that results in the most active surface could be a thin layer, for example nanoparticles that transform into an activated core-shell structure.<sup>72</sup> In contrast, a complete transformation throughout the entire materials' depth may be favorable for highly porous materials.<sup>74</sup> For bimetallic or multi-metallic based materials, some of the metal cations may be chosen to preferentially leach and leave behind a more active undercoordinated metal cation.<sup>75</sup> For example in the case of perovskites, leaching of the metal Asite cations expose more undercoordinated metal B-sites to favor adsorption of OER intermediates.<sup>29</sup> Other approaches may exploit a certain kind of surface defect—like a distinct surface termination, step, edge, kink, grain boundary, or dopant—to facilitate the transformation process toward the final active surface. 73 However, the activity of edge defects, and their propensity for driving surface reconstructions has yet to be determined. Heterostructures, or materials with dissimilar electronic locales, have localized differences in charge transfer which can also impact the resulting transformed surface. 84 The rationale for pre-catalyst starting material should be paired with an appropriate method to induce surface transformation.

Methods to induce surface transformations using external stimuli are sometimes referred to as activation processes. Herein, we focus primarily on electrochemical activation processes,

PLEASE CITE THIS ARTICLE AS DOI: 10.1063/5.0139558

though other less widely used methods include magnetic fields or photo-thermal methods.<sup>75</sup> The extent of transformation or the exact nature of the transformation pathway can differ for various electrochemical activation processes. 85 The linear potential waveform applied during CV is most frequently used. After the cyclic voltammogram continuously overlaps with previous cycles, the material is considered to reach its steady-state condition. However, applying a constant anodic potential (CA) or passing a constant charge (CP) as a function of time means the electrocatalyst only experiences oxidation processes (in the case of OER). When the corresponding current or potential reaches a steady-state value, the electrocatalyst is considered at its steady-state condition. In addition, applying a pulsed potential waveform (CA) or modulating the charge passed per unit time (CP) could cause surface transformations that differ from other electrochemical methods. The frequency of the potential pulse adds another experimental variable that can be tuned.

Rationally designing pre-catalyst materials involves a combination of synthesis, processing, and activation steps. Collaborations between experimental and computational research groups can streamline this process. To achieve the goal of effective pre-catalyst materials, we require detection methods capable of providing information about physical, chemical, and electronic changes happening on the surface with high spatial, temporal, and potential/current resolution.

Bridging the gap between current and future capabilities: Tools for studying electrocatalyst surface transformations

A recurring theme of several recent reviews on OER electrocatalyst surface transformations, <sup>29, 32, 52, 71, 72, 75, 84, 86, 87</sup> proposed transformation mechanisms based on theory, <sup>74, 79,</sup> <sup>81</sup> and experimental methods for detecting surface transformations, <sup>52, 70, 73, 88-90</sup> is a call for future systematic study design. Adhering to reported best practices in the literature, as well as successfully isolating a single experimental variable to study systematically is necessary. For

PLEASE CITE THIS ARTICLE AS DOI: 10.1063/5.0139558

example, a systematic study of surface transformations may focus on the OER mechanism, pHdependence, cation effects, or electrocatalyst subsurface depending on the primary research questions.

Isotopic oxygen labelling and pH studies are two strategies that can deduce whether an electrocatalyst operates via the conventional adsorbate evolution mechanism (AEM), where adsorbates are chemisorbed on metal active sites, or the lattice oxygen mechanism (LOM), where oxygen atoms interact with adsorbates. Lee et al. (2019) used in situ Raman to observe <sup>18</sup>O exchange on and surface oxidation of Ni and NiCo layered double hydroxides (LDHs). 91 Pristine Ni and NiCo LDHs were labelled in <sup>18</sup>O-labeled 0.1 M KOH by holding the working electrode at 1.65 V versus RHE for 3 min, upon which characteristic  $\delta(Ni^{III} - 0)$ ,  $\nu(Ni^{III} - 0)$ , and  $\nu(0 - 0)$ vibrational modes shifted to lower wavenumbers. 91 After reintroduction to 16O-labelled 0.1 M KOH, the Raman bands gradually shifted back to the original wavenumbers in <sup>16</sup>O-labelled electrolyte, indicating lattice oxygen participation in OER on the two surfaces. In contrast, NiFe and NiFeCo LDHs—while highly active for OER—did not demonstrate <sup>18</sup>O exchange, suggesting the increase in activity cannot be explained by a lattice oxygen-mediated mechanism.<sup>91</sup>

Recently, there has been significant progress in understanding trends of perovskite surface stability, <sup>29, 92, 93</sup> particularly related to reaction mechanism and electrocatalyst electronic structure. Online electrochemical mass spectrometry (OLEMS) is another powerful in situ technique used to track isotopically-labelled lattice oxygen during OER. Perovskite oxides A<sub>x</sub>CoO<sub>3-δ</sub> (with A varied from La to Sr) were labelled with <sup>18</sup>O and measured in <sup>16</sup>O-labelled 0.1 M KOH during OLEMS experiments.<sup>26</sup> The LaCoO<sub>3</sub> produced no <sup>36</sup>O<sub>2</sub> (indicative of AEM), while SrCoO<sub>3-δ</sub> produced a significant amount of <sup>36</sup>O<sub>2</sub> (indicative of LOM). <sup>26</sup> However, the relationship between surface transformation and OER mechanism is not yet well defined. For example, <sup>18</sup>O-labelled BSCF82

PLEASE CITE THIS ARTICLE AS DOI: 10.1063/5.0139558

which exhibits a high degree of surface amorphization, <sup>12</sup> evolved only <sup>34</sup>O<sub>2</sub>, and <sup>36</sup>O<sub>2</sub> release did not correspond to OER current.26

Varying electrolyte pH is another way to probe the OER mechanism and distinguish between concerted and non-concerted proton coupled electron transfer. 26 Perovskites with nonconcerted proton-electron transfer that operate by the LOM have pH-dependent kinetics in alkaline electrolytes.  $^{26,29}$  A pH study of Si-doped  $SrCoO_{3-\delta}$  found that the specific activity of OER increased with pH (KOH electrolytes of pH 12.5 to 14.0), suggestive of LOM, and noted that a surface oxygen vacancy formation rate that exceeds the refilling rate explains surface transformation of the perovskite. <sup>18</sup> At neutral pH, all perovskites with O p-bands close to the Fermi level undergo A-site leaching and surface amorphization, but those with O p-bands far from the Fermi level exhibit differences in B-site leaching for two distinct regimes: B-site metal cations leach under high OER current/potentials but not for OER at low current/potentials. 92 Generally, cation leaching from perovskites is more pronounced in neutral electrolytes compared to alkaline electrolytes because the overpotential required to produce a given current density is greater. 92 The local environment near the catalyst-electrolyte interface depends on the applied current/voltage and electrolyte buffering capacity, which both impact local pH gradients.94 High OER rates decrease the local pH in the electrochemical double layer and provide a driving force for dissolution of some metal cations. Thoroughly understanding the interfacial pH and its gradients can improve this theory by clarifying the local pH near the electrocatalyst during OER conditions.95

In addition to electrolyte pH, cations in the electrolyte can be involved in the surface transformation process. Cations in the electrolyte may stabilize the surface, form a passivating layer, increase the propensity for cation dissolution, or alter the OER mechanism. For example,

PLEASE CITE THIS ARTICLE AS DOI: 10.1063/5.0139558

 $La_{0.7}Sr_{0.3}CoO_3$  was only found to show pH-dependent activity when a trace amount of Fe was incorporated into the electrolyte, which was attributed to the interaction of  $Fe_{(aq)}$  and the reconstructed  $CoO_xH_y$  surface and prevention of further dissolution. <sup>96</sup> Improvements in calculated Pourbaix diagrams from first principles by including electrolyte cation effects can provide excellent computational analog to experimental cation studies.

Epitaxial oxide heterostructures can give insight into how the subsurface modifies the electronic and configurational properties of the surface. Electronic and configurational effects, can be controlled by the identity of the substrate material and subsurface oxide layers. These electronic and configurational effects may be leveraged to trigger a desired surface transformation. Modifying the substructure changes in the electronic environment of the surface, and changes the chemical nature of the surface, and lead to increased electrocatalytic activity. In bimetallic systems, this is sometimes referred to as the ligand effect. For example, modifying the substructure of Pt(111) from Ni to Ti caused the d-band to broaden and shift to lower average energies. Other substrate effects include strain and its relaxation. Epitaxial thin films provide an excellent opportunity to study these variables, where substrate lattice mismatch can tune lattice strain and film thickness can be used to produce defects during strain relaxation processes. A substrate often has the role of facilitating electron transport, but can also serve as a sink to modify the electrocatalyst surface. The substrate effects are insight in the substrate often has the role of facilitating electron transport, but can also serve as a sink to modify

In addition to systematic study designs, we draw attention to the importance of accurate interpretation of measured electrocatalyst activity. It is well known that accurate benchmarking of electrocatalysts depends on the method for current normalization. <sup>10, 98</sup> As the electrocatalyst surface transforms during OER, it is especially important to account for changes in the active surface area. This issue raises a question: Does increased OER activity arise from an increased

PLEASE CITE THIS ARTICLE AS DOI: 10.1063/5.0139558

number of active sites on the transformed surface and/or an increased intrinsic activity of those active sites? Whenever possible, it is best practice to employ surface area measurements before and after OER to understand how to appropriately normalize the current obtained from electrochemical measurements.

Electrochemical methods for surface area determination include electrochemical active surface area (ECSA) and electrochemical impedance spectroscopy (EIS). ECSA gives information about the surface area in contact with the electrolyte and is determined using CV at varying scan rates over a potential window with no faradaic processes. 98,99 However, it may be more appropriate to assess changes in the electrocatalyst capacitance before and after OER rather than calculate ECSA because it may be difficult to accurately identify the value of specific capacitance. 100 A comparative study by Zankowski et al. (2019) found that measuring the ECSA via double layer capacitance using EIS at potentials past the OER onset is an accurate way to quantify the ECSA of the electrocatalyst under operating conditions.<sup>101</sup> ECSA is especially appropriate for high surface area electrocatalysts, where geometric area usually underestimates the surface area and leads to normalized currents that overestimate the actual current density. For example, ECSA was used to characterize the FeCoNi-dichalcogenide nanorod array, yielding a surface area 2.92 times greater than that of the Ni-dichalcogenide material alone, demonstrating that incorporation of Fe and Co increased the material's capacitance.<sup>59</sup>

An adsorption-based method for assessing surface area is the Brunauer-Emmett-Teller (BET) surface area measurement via N<sub>2</sub> adsorption and desorption isotherms. This method measures the total physical surface area, not necessarily all the active surface sites, and requires high volumes of electrocatalyst making it an unlikely approach for characterization of transformed surfaces after cycling.

PLEASE CITE THIS ARTICLE AS DOI: 10.1063/5.0139558

A force-based method for assessing surface area is atomic force microscopy (AFM). In this method, the magnitude of the force between a small probe (affixed to a cantilever) and the sample surface is measured by the distance the cantilever is deflected as the probe is scanned across the surface. AFM is most often used to characterize the surface morphology and roughness of model thin films. Single crystals and epitaxial thin films—owing to their low surface roughness, wellcontrolled chemistries and surface terminations, defined crystallographic orientation, and in the case of films, tunable strain—are well suited for surface area characterization using AFM. 102 For films with low surface roughness, it may be acceptable to normalize the measured current by the geometric surface area provided that AFM measurements show little change before and after OER. Additionally, single crystal thin film surfaces are closest to the systems used for DFT modeling, offering the most directly comparable information between experimental and computational studies.103

Given the complexity of surface transformations, a single technique is often insufficient to explain the mechanism of the surface transformation. Each technique usually specializes in specific information. As such, pairing complimentary techniques becomes an important consideration. Most researchers have access to lab-based techniques such as ex situ electron microscopy, FTIR, Raman, XPS, XAS, and XRD, comprising good methods to diagnose if surface changes occur. Some of these lab-based techniques may be amenable to modifications, and researchers can use this to their advantage to develop in-house in situ setups for little expense. For example, integrating Raman spectroscopy and FTIR in the same electrochemical cell provides complimentary information and vibrational modes.<sup>52</sup> A promising avenue of technology development for correlating morphology with adsorbate identity at the solid-liquid interface is electrochemical TERS. 52 Another technology at the development stage is the combination of flow

PLEASE CITE THIS ARTICLE AS DOI: 10.1063/5.0139558

cells with IR and Raman spectroscopy and OLEMS.<sup>52</sup> Recent improvements to surface characterization techniques enable some in situ and operando measurements to probe electrocatalyst surfaces under applied oxidizing potentials, yet limitations still remain. For example, in situ or operando spectroscopy (spectroelectrochemistry) including FTIR and Raman currently lack high temporal resolution. Time-resolved spectroelectrochemical techniques would unlock valuable information about adsorption, surface reaction(s) or interfacial chemical reactions, and desorption of chemical species from the electrified interface to provide detailed insight into reaction mechanisms.<sup>52</sup> Other aspects of spectroelectrochemical setups are membrane electrode assemblies that can be improved by designing electrode supports that do not strongly absorb UVvis-NIR wavelengths.<sup>52</sup> This advance would enable collection of data nearer to commercially relevant conditions. The limitations of each experimental characterization method can motivate the development of new experimental capabilities.

Many options for multimodal characterization techniques are user facilities such as synchrotron sources, which can be accessed via user proposals with a wide range of in situ and operando cells that are unique to each beamline and endstation. Synchrotron facilities have tunable, coherent and bright x-rays (photon flux is  $\sim 10^5 - 10^{10}$  times brighter than lab x-ray tubes<sup>66</sup>). However, in situ (gas phase) and operando (dip-and-pull) lab-based AP-XPS<sup>104</sup> instruments do exist. Synchrotron-based XRD, XAS, and surface-enhanced vibration spectroscopy are useful for observing chemical and structural changes at solid-liquid interfaces, <sup>48</sup> and give information about the electrocatalyst structure, oxidation state, and reaction intermediates.<sup>50, 52</sup> For example, Timoshenko et al. (2022) recently used ex situ TEM, ex situ XPS, in situ XAS at the SuperXAS beamline at the Swiss Light Source synchrotron and operando high energy XRD at the Swiss Materials Science Beamline (P21.2) at PETRA III synchrotron. 105 This combination of

PLEASE CITE THIS ARTICLE AS DOI: 10.1063/5.0139558

experimental characterizations gave information about the morphology, surface electronic structure, oxidation state, and crystal structure, respectively of a Cu-based CO2 reduction reaction electrocatalyst. Another example of a multimodal synchrotron beamline is 11.0.2 at the Advanced Light Source. Beamline 11.0.2 has the capability to perform grazing incidence x-ray scattering and ambient pressure XPS experiments to obtain information about chemical states and adsorbates species at a solid-gas interface at pressures up to the Torr regime.<sup>106</sup> As an electrocatalysis community, it is important to discuss useful combinations of experimental capabilities for future beamlines, and desired capabilities to be incorporated into existing beamlines in the future.

### V. CONCLUSIONS

Surface transformations of electrocatalysts are an emerging focus in the field of heterogeneous electrocatalysis, particularly for the OER during water electrolysis. In this focused review, we detail various detection methods that can be used to understand the electronic and physical origins of electrocatalyst surface transformations that accompanying the OER. Studying the complex nature of surface transformations requires specific probing mechanisms, each with a limited application and scope. 90 In situ and operando techniques are emphasized for observing transformations at or near reaction conditions. Multimodal characterization techniques offer complimentary information to achieve a holistic understanding of complex surface phenomena. Developing tools for accurately interpreting complex transformation dynamics in the context of multiple characterization techniques are also needed.

Many experimental studies focus on the surface transformation process of a single electrocatalyst material, and there remain many open questions. First, it is unclear if the extent of transformation is important to the resulting catalytic activity and structural stability of electrocatalysts.<sup>74</sup> If there is some optimal partial transformation, is it possible to synthesize the appropriate pre-catalyst and design activation processes to target the desired transformation? There

PLEASE CITE THIS ARTICLE AS DOI: 10.1063/5.0139558

are many opportunities to systematically study the role of interfaces, including the substrateelectrocatalyst interface and the electrocatalyst-electrolyte interface.<sup>72</sup> What role do these interfaces play in the surface transformation of OER electrocatalysts? Broadening the scope of these studies to systematically target specific experimental variables, such as OER mechanism, pH-dependence, cation effects, subsurface effects, and electrochemical activation method are strategies that may lead to new insight into new descriptors and trends. Designing studies to answer these research questions will advance the field toward OER electrocatalyst materials for scalable water electrolysis. These research aims will inform the rational design of pre-catalysts and advance water electrolysis technology toward a future of sustainable hydrogen production.

### **AUTHORS' CONTRIBUTIONS**

Molly E. Vitale-Sullivan: writing - original draft (lead); writing - review and editing (equal); visualization (lead). Alvin Chang: conceptualization (supporting); writing - review and editing (supporting). Kuan-Hsun Chou: conceptualization (supporting). Zhenxing Feng: conceptualization (equal); writing - review and editing (equal); supervision (equal); funding acquisition (equal). Kelsey A. Stoerzinger: conceptualization (equal); writing - review and editing (equal); supervision (equal); funding acquisition (equal).

### ACKNOWLEDGEMENTS

This work is supported by National Science Foundation (NSF) under grant No. CBET-2151049 and ITE-2236036. M. E.V.-S. acknowledges support from the Oregon State University Graduate School as a Provost Fellow. A.C. acknowledges support from the NSF Graduate Research Fellowship Program (GRFP) under award No. 2234662.

### VIII. CONFLICT OF INTERESTS

The authors have no conflicts to disclose.

- 1. T. Terlouw, C. Bauer, R. McKenna and M. Mazzotti, Energy & environmental science 15 (9), 3583-3602 (2022).
- 2. A. K. N. Reddy, M. E. Gamboa-Aldeco and J. O. M. Bockris, *Modern electrochemistry*, 2nd ed. (New York: Plenum Press, New York, 1998).
- 3. B. M. Hunter, H. B. Gray and A. M. Müller, Chemical reviews **116** (22), 14120-14136 (2016).
- M. Chatenet, B. G. Pollet, D. R. Dekel, F. Dionigi, J. Deseure, P. Millet, R. D. Braatz, M.
  Z. Bazant, M. Eikerling, I. Staffell, P. Balcombe, Y. Shao-Horn and H. Schäfer, Chemical
  Society reviews 51 (11), 4583-4762 (2022).
- 5. S. Geiger, O. Kasian, M. Ledendecker, E. Pizzutilo, A. M. Mingers, W. T. Fu, O. Diaz-Morales, Z. Li, T. Oellers, L. Fruchter, A. Ludwig, K. J. J. Mayrhofer, M. T. M. Koper and S. Cherevko, Nature catalysis 1 (7), 508-515 (2018).
- 6. W. Tong, M. Forster, F. Dionigi, S. Dresp, R. Sadeghi Erami, P. Strasser, A. J. Cowan and P. Farràs, Nature Energy **5** (5), 367-377 (2020).
- 7. P. Li, R. Zhao, H. Chen, H. Wang, P. Wei, H. Huang, Q. Liu, T. Li, X. Shi, Y. Zhang, M. Liu and X. Sun, Small (Weinheim an der Bergstrasse, Germany) **15** (13), e1805103-n/a (2019).
- 8. A. J. Bard, L. R. Faulkner and H. S. White, *Electrochemical Methods: Fundamentals and Applications*, 3 ed. (John Wiley & Sons, Ltd, 2022).
- 9. S. W. Boettcher and Y. Surendranath, Nature Catalysis 4 (1), 4-5 (2021).
- 10. C. Wei, R. R. Rao, J. Peng, B. Huang, I. E. L. Stephens, M. Risch, Z. J. Xu and Y. Shao-Horn, Advanced materials (Weinheim) **31** (31), e1806296-n/a (2019).

### PLEASE CITE THIS ARTICLE AS DOI: 10.1063/5.0139558

This is the author's peer reviewed, accepted manuscript. However, the online version of record will be different from this version once it has been copyedited and typeset

- T. Wu, S. Sun, J. Song, S. Xi, Y. Du, B. Chen, W. A. Sasangka, H. Liao, C. L. Gan, G.
  G. Scherer, L. Zeng, H. Wang, H. Li, A. Grimaud and Z. J. Xu, Nature catalysis 2 (9), 763-772 (2019).
- 12. K. J. May, C. E. Carlton, K. A. Stoerzinger, M. Risch, J. Suntivich, Y.-L. Lee, A. Grimaud and Y. Shao-Horn, The Journal of Physical Chemistry Letters **3** (22), 3264-3270 (2012).
- 13. M. Risch, A. Grimaud, K. J. May, K. A. Stoerzinger, T. J. Chen, A. N. Mansour and Y. Shao-Horn, Journal of physical chemistry. C **117** (17), 8628-8635 (2013).
- 14. L. C. Seitz, C. F. Dickens, K. Nishio, Y. Hikita, J. Montoya, A. Doyle, C. Kirk, A. Vojvodic, H. Y. Hwang, J. K. Norskov and T. F. Jaramillo, Science **353** (6303), 1011-1014 (2016).
- O. Diaz-Morales, S. Raaijman, R. Kortlever, P. J. Kooyman, T. Wezendonk, J. Gascon,
  W. T. Fu and M. T. M. Koper, Nature Communications 7 (1), 12363 (2016).
- B. Han, A. Grimaud, L. Giordano, W. T. Hong, O. Diaz-Morales, L. Yueh-Lin, J.
  Hwang, N. Charles, K. A. Stoerzinger, W. Yang, M. T. M. Koper and Y. Shao-Horn, Journal of physical chemistry. C 122 (15), 8445-8454 (2018).
- 17. J. Edgington, N. Schweitzer, S. Alayoglu and L. C. Seitz, Journal of the American Chemical Society **143** (26), 9961-9971 (2021).
- Y. Pan, X. Xu, Y. Zhong, L. Ge, Y. Chen, J.-P. M. Veder, D. Guan, R. O'Hayre, M. Li,
  G. Wang, H. Wang, W. Zhou and Z. Shao, Nature communications 11 (1), 2002-2002 (2020).
- 19. K. Schweinar, B. Gault, I. Mouton and O. Kasian, The journal of physical chemistry letters **11** (13), 5008-5014 (2020).

# This is the author's peer reviewed, accepted manuscript. However, the online version of record will be different from this version once it has been copyedited and typeset PLEASE CITE THIS ARTICLE AS DOI: 10.1063/5.0139558

- 21. G. Wan, J. W. Freeland, J. Kloppenburg, G. Petretto, J. N. Nelson, D.-Y. Kuo, C.-J. Sun, J. Wen, J. T. Diulus, G. S. Herman, Y. Dong, R. Kou, J. Sun, S. Chen, K. M. Shen, D. G. Schlom, G.-M. Rignanese, G. Hautier, D. D. Fong, Z. Feng, H. Zhou and J. Suntivich, Science advances 7 (2) (2021).
- K. Fan, H. Zou, Y. Lu, H. Chen, F. Li, J. Liu, L. Sun, L. Tong, M. F. Toney, M. Sui and
  J. Yu, ACS nano 12 (12), 12369-12379 (2018).
- S. H. Chang, N. Danilovic, K.-C. Chang, R. Subbaraman, A. P. Paulikas, D. D. Fong, M.
  J. Highland, P. M. Baldo, V. R. Stamenkovic, J. W. Freeland, J. A. Eastman and N. M.
  Markovic, Nature communications 5 (1), 4191-4191 (2014).
- 24. B. Hammer and J. K. Norskov, Nature (London) **376** (6537), 238-240 (1995).
- 25. J. Suntivich, K. J. May, H. A. Gasteiger, J. B. Goodenough and Y. Shao-Horn, Science (American Association for the Advancement of Science) **334** (6061), 1383-1385 (2011).
- 26. A. Grimaud, O. Diaz-Morales, B. Han, W. T. Hong, Y.-L. Lee, L. Giordano, K. A. Stoerzinger, M. T. M. Koper and Y. Shao-Horn, Nature chemistry **9** (5), 457-465 (2017).
- Y. Sun, H. Liao, J. Wang, B. Chen, S. Sun, S. J. H. Ong, S. Xi, C. Diao, Y. Du, J.-O.
  Wang, M. B. H. Breese, S. Li, H. Zhang and Z. J. Xu, Nature catalysis 3 (7), 554-563 (2020).
- 28. D.-Y. Kuo, H. Paik, J. Kloppenburg, B. Faeth, K. M. Shen, D. G. Schlom, G. Hautier and J. Suntivich, Journal of the American Chemical Society **140** (50), 17597-17605 (2018).
- 29. J.-W. Zhao, Z.-X. Shi, C.-F. Li, Q. Ren and G.-R. Li, ACS materials letters **3** (6), 721-737 (2021).

# This is the author's peer reviewed, accepted manuscript. However, the online version of record will be different from this version once it has been copyedited and typeset. PLEASE CITE THIS ARTICLE AS DOI: 10.1063/5.0139558

- 30. K. A. Stoerzinger, R. R. Rao, X. R. Wang, W. T. Hong, C. M. Rouleau and Y. Shao-Horn, Chem **2** (5), 668-675 (2017).
- 31. L. Giordano, B. Han, M. Risch, W. T. Hong, R. R. Rao, K. A. Stoerzinger and Y. Shao-Horn, Catalysis today **262**, 2-10 (2016).
- 32. H. Ding, H. Liu, W. Chu, C. Wu and Y. Xie, Chemical Reviews **121** (21), 13174-13212 (2021).
- 33. Z. Zeng, M. K. Y. Chan, Z.-J. Zhao, J. Kubal, D. Fan and J. Greeley, Journal of physical chemistry. C **119** (32), 18177-18187 (2015).
- 34. H. D. Espinosa, R. A. Bernal and T. Filleter, Small (Weinheim an der Bergstrasse, Germany) **8** (21), 3233-3252 (2012).
- 35. C. Han, M. T. Islam and C. Ni, ACS omega **6** (10), 6537-6546 (2021).
- 36. I. MacLaren and Q. M. Ramasse, International materials reviews **59** (3), 115-131 (2014).
- 37. T. Tarnev, S. Cychy, C. Andronescu, M. Muhler, W. Schuhmann and Y. T. Chen, Angewandte Chemie (International ed.) **59** (14), 5586-5590 (2020).
- 38. L. A. Giannuzzi, *Introduction to focused ion beams: instrumentation, theory, techniques and practice.* (Springer Science & Business Media, 2004).
- 39. S. Bals, W. Tirry, R. Geurts, Z. Yang and D. Schryvers, Microscopy and microanalysis 13 (2), 80-86 (2007).
- 40. G. Dunn, V. P. Adiga, T. Pham, C. Bryant, D. J. Horton-Bailey, J. N. Belling, B. LaFrance, J. A. Jackson, H. R. Barzegar, J. M. Yuk, S. Aloni, M. F. Crommie and A. Zettl, ACS nano 14 (8), 9637-9643 (2020).
- 41. H. Zheng, R. K. Smith, Y.-w. Jun, C. Kisielowski, U. Dahmen and A. P. Alivisatos, Science (American Association for the Advancement of Science) **324** (5932), 1309-1312 (2009).

# This is the author's peer reviewed, accepted manuscript. However, the online version of record will be different from this version once it has been copyedited and typeset PLEASE CITE THIS ARTICLE AS DOI: 10.1063/5.0139558

- 42. A. J. Leenheer, J. P. Sullivan, M. J. Shaw and C. T. Harris, Journal of microelectromechanical systems **24** (4), 1061-1068 (2015).
- 43. J. P. Patterson, Y. Xu, M.-A. Moradi, N. A. J. M. Sommerdijk and H. Friedrich, Accounts of Chemical Research **50** (7), 1495-1501 (2017).
- 44. D. Mierwaldt, V. Roddatis, M. Risch, J. Scholz, J. Geppert, M. E. Abrishami and C. Jooss, Advanced Sustainable Systems 1 (12), 1700109-n/a (2017).
- 45. S. Hwang, X. Chen, G. Zhou and D. Su, Advanced Energy Materials **10** (11), 1902105 (2020).
- 46. B. C. Garrett, D. A. Dixon, D. M. Camaioni, D. M. Chipman, M. A. Johnson, C. D. Jonah, G. A. Kimmel, J. H. Miller, T. N. Rescigno, P. J. Rossky, S. S. Xantheas, S. D. Colson, A. H. Laufer, D. Ray, P. F. Barbara, D. M. Bartels, K. H. Becker, K. H. Bowen, S. E. Bradforth, I. Carmichael, J. V. Coe, L. R. Corrales, J. P. Cowin, M. Dupuis, K. B. Eisenthal, J. A. Franz, M. S. Gutowski, K. D. Jordan, B. D. Kay, J. A. LaVerne, S. V. Lymar, T. E. Madey, C. W. McCurdy, D. Meisel, S. Mukamel, A. R. Nilsson, T. M. Orlando, N. G. Petrik, S. M. Pimblott, J. R. Rustad, G. K. Schenter, S. J. Singer, A. Tokmakoff, L.-S. Wang and T. S. Zwier, Chem. Rev 105 (1), 355-390 (2005).
- 47. D. Nicholls, J. Lee, H. Amari, A. J. Stevens, B. L. Mehdi and N. D. Browning, Nanoscale **12** (41), 21248-21254 (2020).
- 48. J. Hwang, R. R. Rao, L. Giordano, Y. Katayama, Y. Yu and Y. Shao-Horn, Science (American Association for the Advancement of Science) **358** (6364), 751-756 (2017).
- 49. Y. Chen, Y. Sun, M. Wang, J. Wang, H. Li, S. Xi, C. Wei, P. Xi, G. E. Sterbinsky, J. W. Freeland, A. C. Fisher, J. W. Ager, Z. Feng and Z. J. Xu, Science Advances **7** (50), eabk1788.

# This is the author's peer reviewed, accepted manuscript. However, the online version of record will be different from this version once it has been copyedited and typeset. PLEASE CITE THIS ARTICLE AS DOI: 10.1063/5.0139558

- 50. Y. Wang and D. Chen, ACS Applied Materials & Interfaces **14** (20), 23033-23055 (2022).
- 51. C. R. Brundle, C. A. Evans and S. Wilson, *Encyclopedia of materials characterization : surfaces, interfaces, thin films.* (Butterworth-Heinemann, Boston, 1992).
- 52. A. S. Malkani, J. Anibal, X. Chang and B. Xu, iScience 23 (12), 101776-101776 (2020).
- 53. A. J. Bard and L. R. Faulkner, Russian journal of electrochemistry **38** (12), 1364-1365 (2002).
- 54. Z. Xu, Z. Liang, W. Guo and R. Zou, Coordination chemistry reviews **436**, 213824 (2021).
- 55. B. S. Yeo and A. T. Bell, Journal of the American Chemical Society **133** (14), 5587-5593 (2011).
- 56. X. Wang and L. Guo, Angewandte Chemie (International ed.) **59** (11), 4231-4239 (2020).
- 57. S. Zaleski, A. J. Wilson, M. Mattei, X. Chen, G. Goubert, M. F. Cardinal, K. A. Willets and R. P. Van Duyne, Accounts of chemical research **49** (9), 2023-2030 (2016).
- 58. A. Cuesta, Current opinion in electrochemistry **35**, 101041 (2022).
- 59. Q. Chen, Y. Fu, J. Jin, W. Zang, X. Liu, X. Zhang, W. Huang, Z. Kou, J. Wang, L. Zhou and L. Mai, Journal of energy chemistry 55, 10-16 (2021).
- 60. M. Wang, Q. Wa, X. Bai, Z. He, W. S. Samarakoon, Q. Ma, Y. Du, Y. Chen, H. Zhou, Y. Liu, X. Wang and Z. Feng, JACS Au 1 (12), 2216-2223 (2021).
- M. W. Louie and A. T. Bell, Journal of the American Chemical Society 135 (33), 12329-12337 (2013).
- 62. V. Chakrapani, Frontiers in chemistry **8**, 327-327 (2020).

### PLEASE CITE THIS ARTICLE AS DOI: 10.1063/5.0139558

This is the author's peer reviewed, accepted manuscript. However, the online version of record will be different from this version once it has been copyedited and typeset.

- 63. C. R. Brundle and A. D. Baker, *Electron spectroscopy: theory, techniques, and applications.* (Academic Press, London;, 1977).
- 64. M. Wang and Z. Feng, Current opinion in electrochemistry **30**, 100803 (2021).
- 65. M. Wang, L. Árnadóttir, Z. J. Xu and Z. Feng, Nano-Micro Lett 11 (1), 1-18 (2019).
- 66. F. Frati, M. O. J. Y. Hunault and F. M. F. de Groot, Chemical Reviews **120** (9), 4056-4110 (2020).
- 67. C. Baeumer, J. Li, Q. Lu, A. Y.-L. Liang, L. Jin, H. P. Martins, T. Duchoň, M. Glöß, S.
- M. Gericke, M. A. Wohlgemuth, M. Giesen, E. E. Penn, R. Dittmann, F. Gunkel, R. Waser, M.
- Bajdich, S. Nemšák, J. T. Mefford and W. C. Chueh, Nature Materials 20 (5), 674-682 (2021).
- 68. K. A. Stoerzinger, R. Comes, S. R. Spurgeon, S. Thevuthasan, K. Ihm, E. J. Crumlin and
- S. A. Chambers, The journal of physical chemistry letters **8** (5), 1038-1043 (2017).
- 69. S. H. Chang, J. G. Connell, N. Danilovic, R. Subbaraman, K.-C. Chang, V. R. Stamenkovic and N. M. Markovic, Faraday discussions **176**, 125-133 (2015).
- 70. B. F. Baggio and Y. Grunder, Annual review of analytical chemistry (Palo Alto, Calif.) **14** (1), 87-107 (2021).
- 71. Z. Kou, X. Li, L. Zhang, W. Zang, X. Gao and J. Wang, Small science **1** (7), 2100011-n/a (2021).
- 72. J. Liu and L. Guo, Matter 4 (9), 2850-2873 (2021).
- 73. W. Shen, J. Yin, J. Jin, Y. Hu, H. Yichao, J. Xiao, Y.-Q. Zhao and P. Xi, Advanced Energy and Sustainability Research (2022).
- 74. X. Liu, J. Meng, J. Zhu, M. Huang, B. Wen, R. Guo and L. Mai, Advanced materials (Weinheim) **33** (32), 2007344-n/a (2021).

### PLEASE CITE THIS ARTICLE AS DOI: 10.1063/5.0139558

This is the author's peer reviewed, accepted manuscript. However, the online version of record will be different from this version once it has been copyedited and typeset

- 75. L. Gao, X. Cui, C. D. Sewell, J. Li and Z. Lin, Chemical Society reviews **5** (15), 8428-8469 (2021).
- Y. Zhu, H.-C. Chen, C.-S. Hsu, T.-S. Lin, C.-J. Chang, S.-C. Chang, L.-D. Tsai and H.
  M. Chen, ACS energy letters 4 (4), 987-994 (2019).
- 77. T. Wu, S. Sun, J. Song, S. Xi, Y. Du, C. Bo, W. A. Sasangka, H. Liao, C. L. Gan, G. G. Scherer, L. Zeng, H. Wang, H. Li, A. Grimaud and Z. J. Xu, (Nature Publishing Group, 2019), Vol. 2, pp. 763-772.
- 78. E. Fabbri, M. Nachtegaal, T. Binninger, X. Cheng, B.-J. Kim, J. Durst, F. Bozza, T. Graule, R. Schäublin, L. Wiles, M. Pertoso, N. Danilovic, K. E. Ayers and T. J. Schmidt, Nature materials **16** (9), 925-931 (2017).
- 79. Z.-J. Zhao, S. Liu, S. Zha, D. Cheng, F. Studt, G. Henkelman and J. Gong, Nature reviews. Materials 4 (12), 792-804 (2019).
- 80. S. Samira, J. Hong, J. C. A. Camayang, K. Sun, A. S. Hoffman, S. R. Bare and E. Nikolla, JACS Au 1 (12), 2224-2241 (2021).
- 81. X. Rong, J. Parolin and A. M. Kolpak, ACS catalysis 6 (2), 1153-1158 (2016).
- 82. I. E. L. Stephens, A. S. Bondarenko, F. J. Perez-Alonso, F. Calle-Vallejo, L. Bech, T. P. Johansson, A. K. Jepsen, R. Frydendal, B. P. Knudsen, J. Rossmeisl and I. Chorkendorff, Journal of the American Chemical Society **133** (14), 5485-5491 (2011).
- 83. M. Escudero-Escribano, P. Malacrida, M. H. Hansen, U. G. Vej-Hansen, A. Velazquez-Palenzuela, V. Tripkovic, J. Schiotz, J. Rossmeisl, I. E. L. Stephens and I. Chorkendorff, Science (American Association for the Advancement of Science) **352** (6281), 73-76 (2016).
- 84. J. Chen, H. Chen, T. Yu, R. Li, Y. Wang, Z. Shao and S. Song, Electrochemical energy reviews 4 (3), 566-600 (2021).

# This is the author's peer reviewed, accepted manuscript. However, the online version of record will be different from this version once it has been copyedited and typeset. PLEASE CITE THIS ARTICLE AS DOI: 10.1063/5.0139558

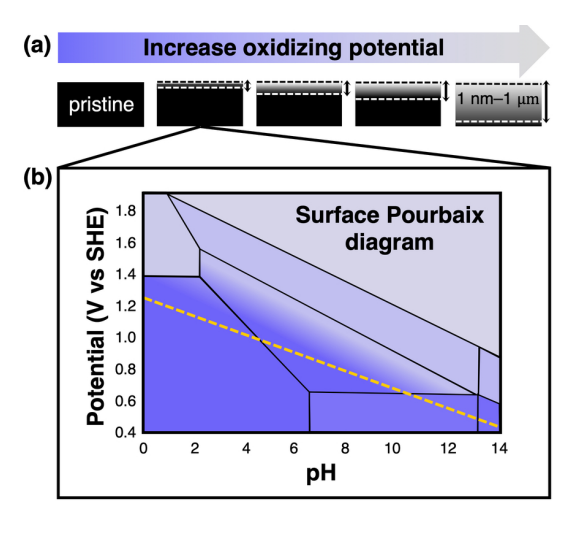
- 85. Y. Zeng, M. Zhao, Z. Huang, W. Zhu, J. Zheng, Q. Jiang, Z. Wang and H. Liang, Advanced energy materials **12** (33), n/a (2022).
- 86. D. A. Kuznetsov, B. Han, Y. Yu, R. R. Rao, J. Hwang, Y. Román-Leshkov and Y. Shao-Horn, Joule **2** (2), 225-244 (2018).
- 87. G. Wan, G. Zhang, J. Z. Chen, M. F. Toney, J. T. Miller and C. J. Tassone, ACS catalysis **12** (13), 8007-8018 (2022).
- 88. H. Sun and W. Zhou, Energy & fuels **35** (7), 5716-5737 (2021).
- 89. V. M. V and G. Nageswaran, Frontiers in chemistry **8**, 23-23 (2020).
- 90. Y. Zhu, J. Wang, H. Chu, Y.-C. Chu and H. M. Chen, ACS energy letters **5** (4), 1281-1291 (2020).
- 91. S. Lee, K. Banjac, M. Lingenfelder and X. Hu, Angewandte Chemie (International ed.) **58** (30), 10295-10299 (2019).
- 92. B. Han, M. Risch, Y.-L. Lee, C. Ling, H. Jia and Y. Shao-Horn, Physical chemistry chemical physics: PCCP 17 (35), 22576-22580 (2015).
- 93. Y. Sun, R. Li, X. Chen, J. Wu, Y. Xie, X. Wang, K. Ma, L. Wang, Z. Zhang, Q. Liao, Z. Kang and Y. Zhang, Advanced energy materials 11 (12), 2003755-n/a (2021).
- 94. I. Katsounaros, S. Cherevko, A. R. Zeradjanin and K. J. J. Mayrhofer, Angewandte Chemie (International ed.) **53** (1), 102-121 (2014).
- 95. M. C. O. Monteiro and M. T. M. Koper, Current opinion in electrochemistry **25**, 100649 (2021).
- 96. P. P. Lopes, D. Y. Chung, X. Rui, H. Zheng, H. He, P. Farinazzo Bergamo Dias Martins, D. Strmcnik, V. R. Stamenkovic, P. Zapol, J. F. Mitchell, R. F. Klie and N. M. Markovic, Journal of the American Chemical Society **143** (7), 2741-2750 (2021).

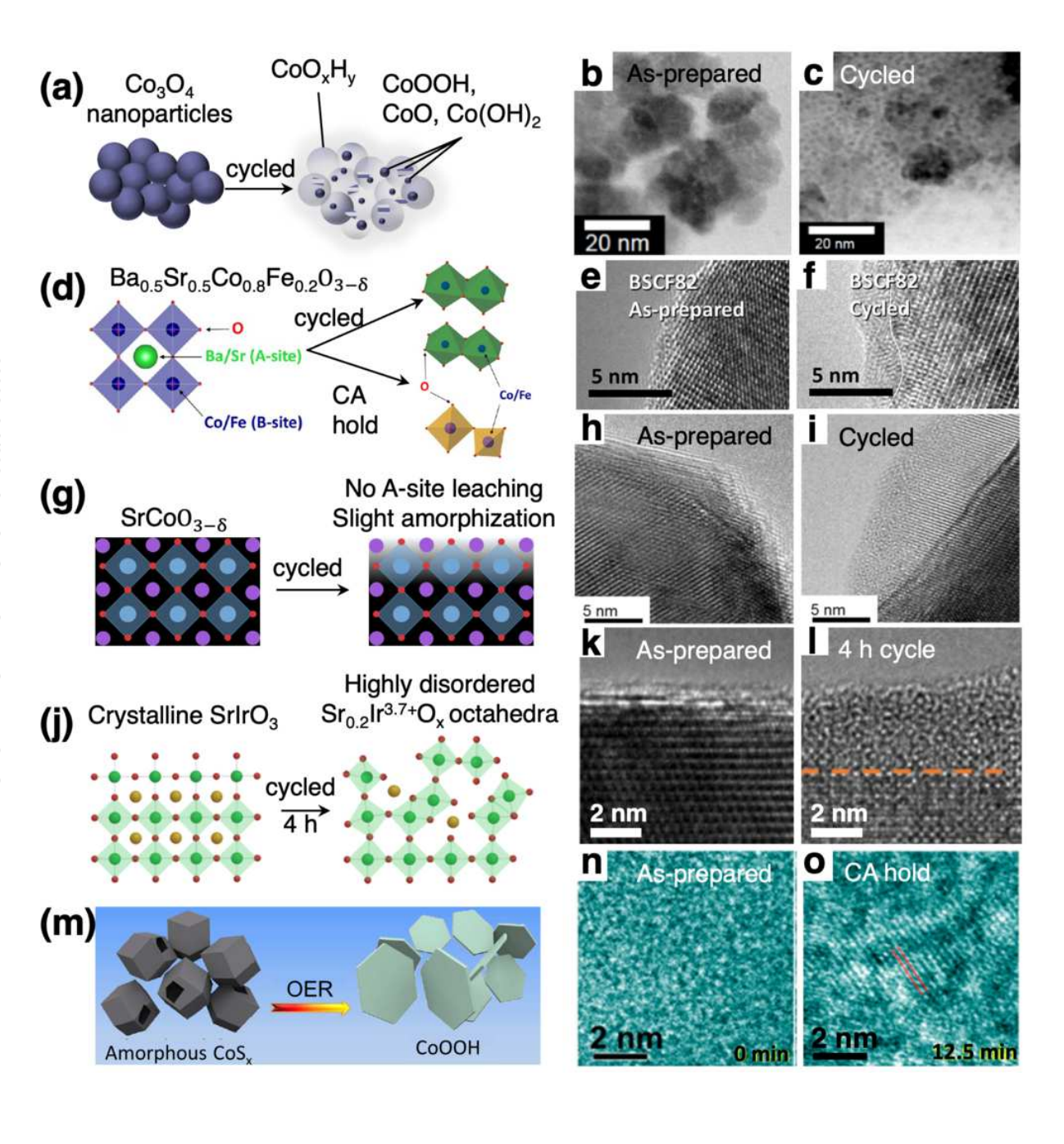
- 100. C. C. L. McCrory, S. Jung, J. C. Peters and T. F. Jaramillo, Journal of the American Chemical Society 135 (45), 16977-16987 (2013).
- 101. S. P. Zankowski and P. M. Vereecken, Journal of the Electrochemical Society 166 (6), D227-D235 (2019).
- P. Adiga and K. A. Stoerzinger, Journal of Vacuum Science & Technology A: Vacuum, Surfaces, and Films 40 (1), 10801 (2022).
- O. Q. Carvalho, P. Adiga, S. K. Murthy, J. L. Fulton, O. Y. Gutiérrez and K. A. Stoerzinger, iScience 23 (12) (2020).
- L.-W. Wu, C. Liu, Y. Han, Y. Yu, Z. Liu and Y.-F. Huang, Journal of the American Chemical Society 145 (4), 2035-2039 (2023).
- 105. J. Timoshenko, A. Bergmann, C. Rettenmaier, A. Herzog, R. M. Arán-Ais, H. S. Jeon, F. T. Haase, U. Hejral, P. Grosse, S. Kühl, E. M. Davis, J. Tian, O. Magnussen and B. Roldan Cuenya, Nature catalysis 5 (4), 259-267 (2022).
- 106. H. Kersell, P. Chen, H. Martins, Q. Lu, F. Brausse, B.-H. Liu, M. Blum, S. Roy, B. Rude, A. Kilcoyne, H. Bluhm and S. Nemšák, Review of scientific instruments 92 (4), 44102-044102 (2021).

### ACCEPTED MANUSCRIPT

### Chemical Physics Reviews

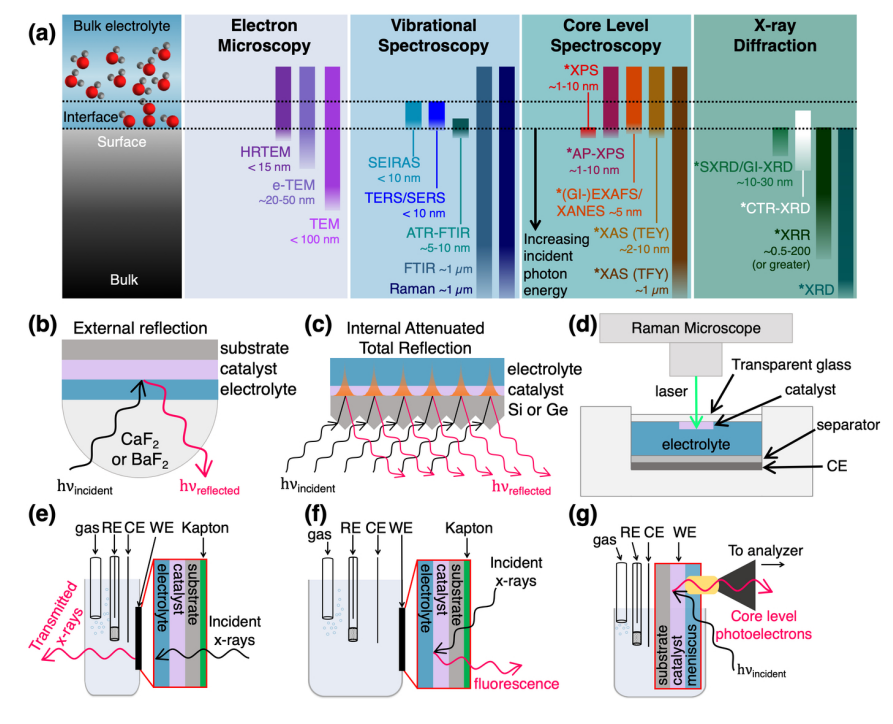
This is the author's peer reviewed, accepted manuscript. However, the online version of record will be different from this version once it has been copyedited and typeset.





### Chemical Physics Reviews

This is the author's peer reviewed, accepted manuscript. However, the online version of record will be different from this version once it has been copyedited and typeset.



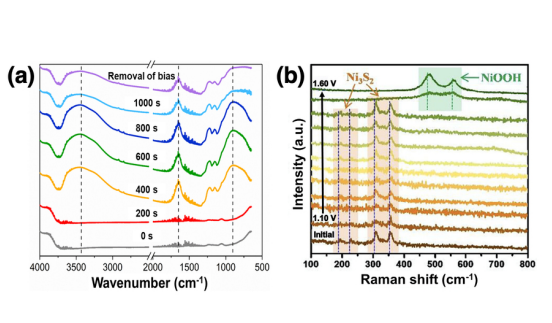




### Chemical Physics Reviews

### ACCEPTED MANUSCRIPT

This is the author's peer reviewed, accepted manuscript. However, the online version of record will be different from this version once it has been copyedited and typeset.



# ACCEPTED MANUSCRIPT

### Chemical Physics Reviews

This is the author's peer reviewed, accepted manuscript. However, the online version of record will be different from this version once it has been copyedited and typeset.

